Numerical Analysis and Experiments on the Acoustics of Conch Shells Modelled as Spiral Cavities

Rasoul Morteza Pouraghdam

A Thesis

in

The Department

of

Mechanical and Industrial Engineering

Presented in Partial Fulfillment of the Requirements

for the Degree of

Master of Applied Science (Mechanical Engineering) at

Concordia University

Montréal, Québec, Canada

July 2016

CONCORDIA UNIVERSITY

School of Graduate Studies

This is to certify that the thesis prepared

By: **Rasoul Morteza Pouraghdam**

Entitled: **Numerical Analysis and Experiments on the Acoustics of Conch Shells Modelled as Spiral Cavities**

and submitted in partial fulfillment of the requirements for the degree of

Master of Applied Science (Mechanical Engineering)

complies with the regulations of this University and meets the accepted standards with respect to originality and quality.

Signed by the Final Examining Committee:

_____ Chair
Dr. Ivan Contreras

_____ External Examiner
Dr. Wei-Ping Zhu

_____ Examiner
Dr. Georgios Vatistas

_____ Supervisor
Dr. Rama B. Bhat

Approved by _____
Martin D. Pugh, Chair
Department of Mechanical and Industrial Engineering

_____ 2016

_____
Amir Asif, Dean
Faculty of Engineering and Computer Science

Abstract

Numerical Analysis and Experiments on the Acoustics of Conch Shells Modelled as Spiral Cavities

Rasoul Morteza Pouraghdam

The wave propagation behavior in spiral cavity of a conch shell is studied. A conch shell consists of a spiral inner cavity where if excited by lip-vibration, a highly resonating sound with harmonic modes is produced. In order to understand how sound is generated in a conch shell, we used X-ray tomography scans to model the shell's unwrapped inner cavity and measured how well the model matches the experimental data.

Experiments were carried out in a semi-anechoic chamber where the conch shell was played using: (i). Lip-excitation (ii). Loudspeaker sine-sweep excitation and (iii). Excitation using an electro-pneumatic transducer. The recorded sounds were analyzed in terms of their frequency components and directivity of the emanating sound.

Moreover, we approximated a shell's inner spiral cavity to a straight tube based on the X-ray data measurements, and to affirm its validity, we compare the resonance modes of the approximated straight tube to the modes recorded from the lip-excited conch shell.

Finally, we study wave propagation in conical and exponential spiral strings and tubes in more general cases, where numerical simulation is carried out whenever the theoretical solutions are hard to find. In the case of the strings, we also computed the resonance modes as well as the time-dependent behaviour.

Acknowledgments

I would like to thank my supervisor, Dr. Rama Bhat for having given me the opportunity to work on this interesting multidisciplinary subject and his guidance throughout the project. I also thank Dan Juras for the technical assistance, as well as Dr. Gary Scavone from McGill University and Dr. Eusebius Doedel from Concordia University for their theoretical inputs and discussions. Finally I want to thank my family especially my parents for their support and encouragement throughout the years.

Contents

List of Figures

List of Tables

Nomenclature

α	Taper factor in 3.1, growth factor in 3.2.2
β	Taper factor in 3.2.2
μ	String linear density, growth factor in 1.9 and 3.1
ν	Damping coefficient in 3.2
ω	Angular frequency
ρ	Density, radius in 1.7 and 3.2
σ	Medium density
c	Wave speed
df	Frequency step
f	Frequency
f_c	Cut-off/Critical frequency
J	Bessel function
k	Wave number
L	Length
m	String segment mass in 1.1, growth factor in 1.5
N	Neumann function

p	Acoustic pressure
Q	Acoustic volume flow
R	Reflected power, mouth radius in 1.7
r_m	End/Mouth radius
r_t	Throat radius
S	Cross-section area
T	Tension, computation duration in 3.2
Z	Acoustic impedance

Chapter 1

Introduction and Literature Review

The core motivation behind this thesis is understanding how sound is generated from the conch shell. The conch shell is one of the earliest brass-like instruments used by mankind, played in different parts of the world for various purposes such as coded communication, signaling purposes and also as a musical instrument. Conch shells are widely used in countries such as in India and Japan during ceremonies and rituals. [1] We first commence by stating the existing acoustic theories on wave propagation along a flexible string and inside cylindrical, conical and exponential tubes/pipes.

1.1 Wave motion along a string

Vibrating strings have been a topic of study for a long time. Pythagoras claimed that if a string is divided into two segments of a particular ratio like 2:1, 3:1 etc. the produced sound by the string is more pleasing to the ear. We know that an excited string produces modes, sometimes referred to as normal modes and they depend upon the string's mass, length, applied tension and also the end conditions (like fixed-open or fixed-fixed). [2] In music a string is excited in different ways, such as by bowing, plucking or striking and thus the string vibration will usually be a combination of several vibration modes. For instance if a string is excited near its center, the resulting resonance spectrum will show a fundamental and only odd integer multiples of that fundamental frequency. However here we will attempt to derive the one-dimensional wave equation by considering an amount of force applied to a string element (figure 1.1). Consider a uniform string with linear density μ being

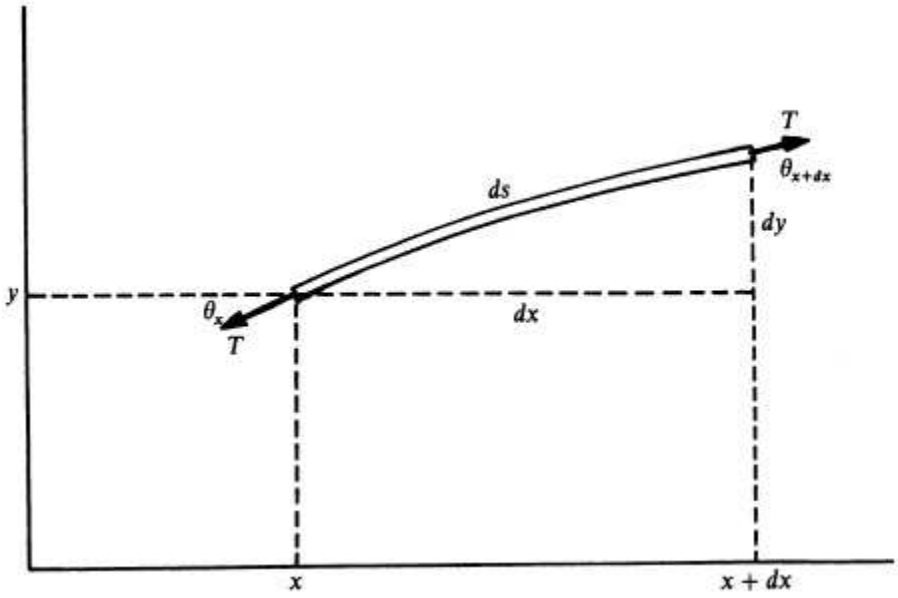

Figure 1.1: String element of length ds subject to a tension T.

subject to a tension T in newtons. There will be a net force dF which restores the string segment dl back to its equilibrium, which is equal to the difference of the tension's y component at the two ends of the string segment:

$$dF_y = (Tsin\theta)_{x+dx} - (Tsin\theta)_x \tag{1}$$

Applying a Taylor's series expansion to the first term in the equation and after simplification we obtain:

$$dF_y = \frac{\partial(Tsin\theta)}{\partial x}dx \tag{2}$$

Since our problem is in a small element scale, we can consider that the displacement in the y direction is small and thus, we have $sin\theta \approx tan\theta = \frac{\partial y}{\partial x}$:

$$dF_y = \frac{T\frac{\partial y}{\partial x}}{\partial x}dx = T\frac{\partial^2 y}{\partial x^2}dx \tag{3}$$

We also have $m = \mu dl$, the string segment mass, and therefore:

$$T\frac{\partial^2 y}{\partial x^2}dx = \mu dl\frac{\partial^2 y}{\partial t^2} \tag{4}$$

Finally by taking $dl \approx dx$ and defining the wave speed as $c = \sqrt{\frac{T}{\mu}}$:

$$\frac{\partial^2 y}{\partial t^2} = \frac{T}{\mu}\frac{\partial^2 y}{\partial x^2} = c^2\frac{\partial^2 y}{\partial x^2} \tag{5}$$

This is known as the wave equation. The general solution to this equation is given by d'Alembert(1717-1783):

$$y = f(ct - x) + g(ct + x) \tag{6}$$

where arbitrary functions f and g represent a wave quantity traveling to the right and left respectively, with a velocity c.

When we refer to resonance modes, it is important to describe the notion of standing waves.

Assuming the wave solution to be harmonic, we have $f(ct-x) = A_1 sin(\omega t - kx) + B_1 sin(\omega t - kx)$ and $g(ct + x) = A_2 sin(\omega t + kx) + B_2 cos(\omega t + kx)$, thus:

$$y = f(ct-x)+g(ct+x) = A_1 sin(\omega t-kx)+B_1 sin(\omega t-kx)+A_2 sin(\omega t+kx)+B_2 cos(\omega t+kx) \tag{7}$$

where $k = \frac{\omega}{c}$ is the wave number.

Considering a string of length L, fixed at both of its ends ($x = 0, x = L$) with the boundary condition $y(x = 0, t) = 0$ implicating that $A_1 = -A_2$ and $B_1 = -B_2$, we have:

$$y = 2A_1 sin(kx)cos(\omega t) - 2B_1 sin(kx)sin(\omega t) = 2sin(kx)[A_1 cos(\omega t) - Bsin(\omega t)] \tag{8}$$

The second boundary condition $y(x = L, t) = 0$ requires the term $sin(kx)$ at $x = L$ to be zero. Therefore $kL = \frac{\omega L}{c} = n\pi$, and therefore $\omega = \frac{n\pi c}{L}$ and since $\omega = 2\pi f$ we have:

$$f_n = \frac{nc}{2L} \tag{9}$$

known as the "modes" of the string, which are also harmonic because all the modes are integer multiples of the fundamental frequency $f = \frac{c}{2L}$ corresponding to $n = 1$.

1.2 Infinite cylindrical tube

In this section we take a look at wave propagation inside an infinite pipe of circular cross section. The wavefronts in such an enclosure is planar and the direction of propagation is along the tube's axis. We also assume the tube's walls to be rigid, perfectly smooth and insulating thus having no effect on wave propagation. A pressure wave (taking the direction of propagation as x) is of the form: $p(x,t) = p_0 e^{j(\omega t - kx)}$. An important quantity regarding wave propagation in tubes is the acoustic volume flow Q, which can be found from $p = \frac{\rho c Q}{S}$ where p is the acoustic pressure, ρ the air density, c the speed of sound in air and S the tube's cross-section area. Therefore we have:

$$Q(x,t) = \frac{pS}{\rho c} e^{j(\omega t - kx)} \tag{10}$$

We can now find the acoustic impedance of the tube from:

$$Z(x) = \frac{p(x,t)}{Q(x,t)} = \frac{\rho c}{S} \tag{11}$$

We now attempt to solve the wave equation for our geometry. Naturally, we would choose to derive the wave equation in cylindrical coordinates (r, Φ, x) where x is basically the height of the cylinder if it is taken to be vertically positioned. Taking the tube's cross-section radius as r_0 with the tube's surface to be rigid, we have $\frac{\partial p}{\partial r}_{r=r_0} = 0$ as the boundary condition on the surface since there is no flow normal to the tube's outer surface. The wave equation in cylindrical coordinates is given as:

$$\frac{\partial^2 p}{\partial r^2} + \frac{1}{r}\frac{\partial p}{\partial r} + \frac{1}{r^2}\frac{\partial^2 p}{\partial \phi^2} + \frac{\partial^2 p}{\partial x^2} = \frac{1}{c^2}\frac{\partial^2 p}{\partial t^2} \tag{12}$$

which has the solution: [3]

$$p_{mn}(r,\phi,x) = p_{sin}^{cos}(m\phi) J_m\left(\frac{\pi q_{mn} r}{r_0}\right) e^{j(\omega t - k_{mn} x)} \tag{13}$$

where J_m is the Bessel function and q_{mn} defined by the boundary condition on the wall so that $J'_m(\pi q_{mn}) = 0$ with integers m and n starting from 0. The (m,n) index indicates the nodal circles

(n) and nodal diameters m of the acoustic pressure. Thus the wave vector k_{mn} is defined as:

$$k_{mn}^2 = (\frac{\omega}{c})^2 - (\frac{\pi q_{mn}}{r_0}) \tag{14}$$

We can see that in the plane mode ($m = n = 0$) we obtain the well known definition of the wave number $k = k_{00} = \frac{\omega}{c}$. For higher modes the angular frequency ω must be larger than the critical value of $\omega_c = \frac{\pi q_{mn} c}{r_0}$.

However since tubes are always of finite length used in real applications, we must cover the case of finite cylindrical tubes.

1.3 Finite cylindrical tubes

In the case of a finite cylindrical pipe, we will have wave reflection from the tube's end (regardless of the end being open or closed). Since in musical applications tubes are mostly coupled to a driver, we can start by finding the input impedance with a finite load impedance Z_L at its end. Consider the tube to be of length L with a terminating impedance $Z_{x=L} = Z_L$. Since the wave quantity is a superposition of two separate quantities travelling to the right and left with a certain amplitude, the wave will be of the form (assuming plane waves only):

$$p(x,t) = Ae^{j(\omega t - kx)} + Be^{j(\omega t + kx)} \tag{15}$$

Using Newton's second law, we know that the pressure and flow in a cylindrical tube are related by:

$$\frac{\partial p}{\partial x} = -\frac{\rho}{S}\frac{\partial Q}{\partial t} \tag{16}$$

From equation 15 we have:

$$jk(Be^{jkx} - Ae^{-jkx})e^{jwt} = -\frac{\rho}{S}\frac{\partial Q}{\partial t} \tag{17}$$

After integration, we obtain:

$$Q(x,t) = \frac{S}{\rho c}[Ae^{j(\omega t - kx)} - Be^{j(\omega t + kx)}] \tag{18}$$

The complex quantity $\frac{B}{A}$ helps define the power reflected from the terminating impedance Z_L. We know by definition that:

$$Z_L = \frac{p(L,t)}{Q(L,t)} \tag{19}$$

And the characteristic wave impedance is defined as:

$$Z_c = \frac{\rho c}{S} \tag{20}$$

It can be found that:

$$\frac{B}{A} = e^{-2jkL}\frac{Z_L - Z_c}{Z_L + Z_c} \tag{21}$$

Thus taking the norm 2 of the complex ratio, we obtain the reflected power:

$$R = \left|\frac{B}{A}\right|^2 = \left|\frac{Z_L - Z_c}{Z_L + Z_c}\right| \tag{22}$$

Depending on the value of Z_L we have either no reflection $R = 0$ ($Z_L = Z_c$) or complete reflection $R = 1$ ($Z_L = 0$ or $Z_L = \infty$). We will also have perfect reflection if Z_L is imaginary but since often Z_L has a non-zero real part, the wave propagation will be lossy.

We now proceed to finding the resonance modes in our system. The impedance at $x = 0$ also known as the input impedance is given by:

$$Z_{IN} = \frac{p(x=0,t)}{Q(x=0,t)} = Z_c\frac{A+B}{A-B} = Z_c\frac{Z_L coskL + jZ_c sinkL}{jZ_L sinkL + Z_c coskL} \tag{23}$$

The expression can be reduced based on the low-frequency approximation, where if $Z_L = 0$ (open end):

$$Z_{IN} = jZ_c tankL \tag{24}$$

And if $Z_L = \infty$ (closed end):

$$Z_{IN} = -jZ_c cotkL \tag{25}$$

It must be noted that the case of $Z_L = 0$ cannot be exactly produced physically. We may now find the resonance frequencies by applying the boundary condition that the input end is also open, more specifically $Z_{IN} = 0$. Thus in the case of the terminated pipe ($Z_L = \infty$), $cotkL = 0$ and thus:

$$\omega^{open-ended} = \frac{(2n-1)\pi c}{2L} \tag{26}$$

which is equivalent to:

$$f^{open-ended} = \frac{(2n-1)c}{4L} \tag{27}$$

corresponding to odd integer multiples of quarter wavelengths, and for an open-open tube we have $tankL = 0$ resulting in:

$$\omega^{open-open} = \frac{n\pi c}{L} \Leftrightarrow f^{open-open} = \frac{nc}{2L} \tag{28}$$

corresponding to integer multiples of the fundamental frequency $f_0 = \frac{c}{2L}$

1.4 Finite conical horn

Horns are usually defined as a closed conduit of larger length compared to its lateral dimensions. [4] We attempt to find the resonance modes inside a finite conical tube of length L. Olson [5] gave the following expression for the input impedance of a conical horn of cross-section area S_1 at $x = x_1$ and S_2 at $x = x_2$ with $L = x_2 - x_1$:

$$Z_{IN} = \frac{\rho c}{S_1} \frac{jZ_L \frac{sink(L-\theta_2)}{sin\theta_2} + \frac{\rho c}{S_2} sinkL}{Z_L \frac{sink(L+\theta_1-\theta_2)}{sin\theta_1 sin\theta_2} - \frac{j\rho c}{S_2} \frac{sink(L+\theta_1)}{sin\theta_1}} \tag{29}$$

with $(\theta_1, \theta_2) = (tan^{-1}kx_1, tan^{-1}kx_2)$. We now examine the input impedance based on the tube's enclosure. For an open end $Z_L = 0$ (either the wide or the narrow end of the tube) we obtain:

$$Z_{IN} = j\frac{\rho c}{S_1}\frac{sinkLsin\theta}{sink(L+\theta_1)} \tag{30}$$

Based on which end is considered to be open, the input impedance will be different since the sign of L and the magnitude of θ_1 will vary. We clearly see that by taking the input impedance zero, $sinkL = 0$ which gives us the set of resonance modes $f = \frac{nc}{2L}$ which is the same as in the case of an open cylindrical tube of length L.

However if $Z_L = \infty$, we have $sink(L + \theta_1) = 0$ which requires:

$$kL + k\theta_1 = n\pi \Leftrightarrow kL = n\pi - tan^{-1}kx_1 \tag{31}$$

For a cone measured from its narrow end (throat), $L > 0$ and $tan^{-1}kx_1 < \frac{\pi}{2}$ we see that the resonance modes are higher than those of a cylinder of equal length L. For a nearly complete tapering cone ($x_2 < x_1$), we have $kx_1 \ll 1$, therefore approximating $tan^{-1}kx_1 \approx kx_1$ and since $L = x_2 - x_1$, from the previous equation we obtain $kx_2 = n\pi$, meaning that the resonance modes are the same as those of an open cylinder of length x_2. We will not cover the case of cones with a termination at the mouth since they're not useful in musical acoustic applications.

1.5 Exponential Horn

Exponential horns make up portions of internal brass instrument bores. We take the radius to be a function of $r = Ae^{mx}$ where m is the growth rate. To come up with the pressure profile inside the horn, we first introduce "Webster's Horn Equation", which in its simplest form can be written as:

$$\frac{1}{S}\frac{\partial}{\partial x}(S\frac{\partial p}{\partial x}) = \frac{1}{c^2}\frac{\partial^2 p}{\partial t^2} \tag{32}$$

where $S(x)$ is the horn's cross-sectional area at distance x. Substituting $p = \psi S^{\frac{1}{2}}$ and assuming simple harmonic motion ($p(x) = \psi(x)e^{j\omega t}$), Webster's equation can be re-written as:

$$\frac{\partial^2 \psi}{\partial x^2} + ((\frac{\omega}{c})^2 - \frac{1}{r}\frac{\partial^2 r}{\partial x^2})\psi = 0 \tag{33}$$

Considering the exponential horn geometry, we have $\frac{1}{r}\frac{\partial^2 r}{\partial x^2} = m^2$ and therefore equation 33 becomes:

$$\frac{\partial^2 \psi}{\partial x^2} + ((\frac{\omega}{c})^2 - m^2)\psi = 0 \tag{34}$$

With a sound pressure profile of the form:

$$p(x) = e^{-mx}e^{j(\omega t - \sqrt{k^2 - m^2 x^2})} \tag{35}$$

with $k = \frac{\omega}{c}$ the wave number. In exponential horns waves can propagate above a cut-off frequency of $f_c = \frac{mc}{2}$ with a dispersive (frequency dependent) phase velocity of $\frac{c}{\sqrt{1-(\frac{\omega_c}{\omega})^2}}$. Below the cut-off frequency the horn transmits nothing with the throat impedance being purely reactive (waves are exponentially damped). Without getting into details, it must be said that exponential horns are efficient sound radiators above the cut-off frequency. Of course exponential horns are not directly used in brass instruments due to lack of resonance modes, however the flared cross-sections in brass instruments enhance sound radiation in the same manner. Exponential horns were widely used in the past, such as in gramophones, amplifying the sound when electronic amplification methods were absent. They are still being used in many public signaling devices as efficient sound detectors with a microphone placed at the horn's apex.

1.6 Conch shell inner cavity approximation by a straight duct

The earliest study on conch shell acoustics was done by Bhat [6] where it was claimed that the conch shell produces a resonating sound if a harmonic of the driver's frequency (lip-vibration) matches the shell's cavity fundamental resonance. In this case the spectrum of the conch sound displayed clear harmonics of a fundamental frequency. Therefore the idea rose that, maybe the inner

spiral cavity can be approximated by a straight tube with increasing cross-sectional area.

Bhat incorporated a very simple measurement to approximate the inner spiral cavity length by measuring the outer surface spiral with a string. The measurement validated the resonance modes, however this study was very preliminary and sought deeper analysis.

Bhat, Taylor and Prasad [7] went further by geometrically modelling the conch shell inner cavity with the help of X-ray tomography scans, in addition to spectrum analysis. They used X-ray scans (Sagittal point of view) to measure the cavity spiral radius at each π turn, as well as the radius-height profile of the spiral. Using the radius-angle data, they were able to fit piecewise conical or Archimedes spirals to the global cavity spiral, and find the total spiral length by integrating piecewise spiral lengths using:

$$L = \int dL = \sqrt{dx^2 + dy^2 + dz^2} \tag{36}$$

where $(dx, dy) = (r\cos(d\theta), r\sin(d\theta))$ with $dz(r)$ being a function of the radius. They obtained a length of $51cm$ on their conch shell sample which was interestingly close to a rough length estimation of a wrapped string around the outer surface of the shell. Then they used the following formula to obtain the theoretical resonance modes of an equivalent conical horn:

$$f_n = \frac{nc}{2(L + 0.6(r_{throat} + r_{mouth}))} \tag{37}$$

However due to the presence of the player's lips the term r_{throat} was neglected. Also since the wave is reflected before the final flare of the horn, the acoustic length of the horn is shorter than the physical length of the tube and thus the term r_{mouth} was safely ignored as well. Using the radii and spiral length data at each π turn, they recreated the major (horizontal) radius-spiral length profile in which they found that the cavity flare begins somewhere near $39cm$ and thus the fundamental frequency of a $39cm$ duct is $f = 440Hz$ (corresponding to the A4 note). This corresponded well with the recorded resonance modes of the shell (approximately $440Hz$ and its harmonics). They claimed that this supports the idea that standing waves reflect back before the final flare of a tube. In chapter two, we provide more details on this procedure in addition to new measurements. Rath and Naik [8] by using X-ray scans discovered that the conch shell geometry contains Fibonacci patterns. The Fibonacci sequence is generated by $f_{n+1} = f_n + f_{n-1}$ with $f_0 = 0$, $f_1 = 1$ and $n = 1, 2, 3, ...$

It is worth nothing that the Fibonacci pattern is also present in many elements of nature such as in plant growth, leaf patterns, floral petals and stems. They found the spiral curve of a nautilus shell to have the formation of a Fibonacci rectangle. They also found that with the proper selection points inside a conch shell cavity, the ratio of the consecutive measurements fall close to the golden ratio ($\frac{\sqrt{5}-1}{2}$). We also verified this finding on our own sample which is explained in chapter 2.

1.7 Conch shell acoustic model - conical spiral cavity geometry

Rath and Naik [9] went further by coming up with a theoretical acoustic model for the conch shell using the recorded resonance modes. They claimed that the conch shell cavity is essentially a wrapped conical horn and thus, acoustic models pertinent to the conical horn may be applied to the conch shell as well. We briefly present their derivations in finding the resonance modes.
For a conical horn it is natural to derive the wave equation in spherical coordinates:

$$\nabla^2 p = \frac{1}{c^2}\frac{\partial^2 p}{\partial t^2} \tag{38}$$

where the radial part of the equation (corresponding to the first term in the Laplacian term) is given by:

$$\frac{\partial^2 P}{\partial \rho^2} = \frac{1}{c^2}\frac{\partial^2 P}{\partial t^2} \tag{39}$$

where $P = \rho p$. By considering the time-independent version of the equation (a.k.a. the Helmholtz Equation) we have:

$$\frac{\partial^2 P}{\partial \rho^2} + k^2 P = 0 \tag{40}$$

where $k = \frac{\omega}{c}$ is the wave number. The solutions to the equation are of the form:

$$P = e^{\pm ik\rho} \Leftrightarrow p = \frac{e^{\pm ik\rho}}{\rho} \tag{41}$$

Applying the boundary condition $p(\rho = \rho_2) = 0$ where ρ_2 corresponds to the open end of the cone, the solution will be of form:

$$p(\rho) = \frac{\sin kl}{\rho} \tag{42}$$

where $l = \rho - \rho_2$. Since the throat is usually driven by lip-excitation, it can be considered as a closed end. We know that in a truncated cone with one closed end (throat) and the mouth being open, the resonance modes fall into the odd harmonics of a closed-open cylinder. In fact, Ayers et al. [10] found that as the ratio of the input to output diameters of a truncated cone increases, the resonance modes deviate from the harmonics of an open-open cylinder, to non-harmonic modes during the transitional regime, and finally to the odd harmonics of a closed-end cylinder of the same length. Therefore, Rath and Naik also argued that since the conch shell is played at the throat where a closed end is considered, the resonance modes in the shell must also be odd harmonics i.e.:

$$f_n = \frac{(2n+1)c}{4l} \tag{43}$$

Based on some simple calculations, they found the shell's effective length to be $l = 4\pi R$ where R is the open end (mouth) radius corresponding to a spiral having a total of 8π turns. Therefore the final expression for the resonance modes is given by:

$$f_n = (2n+1)\frac{c}{16\pi R} \tag{44}$$

However they also recorded the sample conch shell spectrum and found the presence of harmonics of the fundamental mode (both odd and even multiples of the fundamental). However the equation above only suggests the presence of odd multiples of the fundamental mode. The explanation for this phenomenon which they provided is that lip-vibration acts like a sinusoidal vibration then the whole reed plus shell system is simultaneously an open-open and closed-open system, in which case all harmonic modes can be created. However we do want to note that Rath and Naik's explanation may not be always true, considering that many other systems also have non-harmonic resonance modes but can produce harmonic modes when driven by lip-vibration as lip-vibration or reed mechanics in general are highly non-linear.

1.8 Conch shell acoustic model based on Webster's horn equation

In 2010, Rath and Naik [11] came up with a more rigorous conch shell acoustic model based on Webster's horn equation, which we will review on the core points here. Webster's horn equation in its general form is given by [12]:

$$\ddot{\psi} = c^2(\nabla^2\psi + (\vec{\nabla}\psi).\vec{\nabla}(lnS)) \tag{45}$$

As for describing the conch shell cavity geometry, it is wound around the collumella as a growing spiral in the θ and z directions thus the cylindrical coordinate system is applied (ρ, θ, z). They considered the spiral to have the general form of $\rho = k\theta$ in the $x - y$ plane and $h = lz$ being the height of the spiral with growth factors k and l. The central spiral (passing by the center of origin of the cross-section) defined by $\rho = k\theta$, thus the inner and outer spirals being $\rho_{in} = (k - \lambda)\theta$ and $\rho_{out} = (k + \lambda)\theta$, respectively. Thus the varying diameter of the cross-section is obtained by: $d = \rho_{out} - \rho_{in} = 2\lambda\theta$. The spiral length element in the z-direction being defined as $dz = lz$, the cross section radius can be defined as:

$$r^2 = (\lambda\theta)^2 + (lz)^2 \tag{46}$$

and consequently the cross-section area:

$$S = \lambda'\theta^2 + l'z^2 \tag{47}$$

where $\lambda' = \lambda^2$ and $l' = l^2$.

Furthermore, they assumed harmonic motion i.e. $\psi(\rho, \theta, z, t) = \psi(\rho, \theta, z)e^{j\omega t}$. Therefore $\ddot{\psi} = -\omega^2\psi(\rho, \theta, z)$ and Webster's equation can be reduced to:

$$\nabla^2\psi + (\vec{\nabla}\psi).\vec{\nabla}(lnS) = -\frac{\omega^2}{c^2}\psi \tag{48}$$

Then replacing the ∇ operators with the respective expressions in cylindrical coordinates yields:

$$[\frac{1}{\rho}\frac{\partial}{\partial\rho}(\rho\frac{\partial}{\partial\rho}]+\frac{1}{\rho^2}\frac{\partial^2}{\partial\theta^2}+\frac{\partial^2}{\partial z^2}]\psi^2+[\rho\frac{\partial\psi}{\partial\rho}+\frac{\theta}{\rho}\frac{\partial\psi}{\partial\theta}+k\frac{\partial\psi}{\partial z}].[\rho\frac{\partial}{\partial\rho}+\frac{\theta}{\rho}\frac{\partial}{\theta}+l\frac{\partial}{\partial z}]lnS+\frac{\omega^2}{c^2}\psi=0 \quad (49)$$

However they took S to be independent of the variable ρ, thus all the ρ derivatives in the expression above are cancelled out. After further simplification, they obtained:

$$[\frac{1}{\rho}\frac{\partial}{\partial\rho}(\rho\frac{\partial}{\partial\rho}]+\frac{1}{\rho^2}\frac{\partial\psi}{\partial\theta}\frac{2\lambda'\theta}{S}+\frac{\partial\psi}{\partial z}\frac{2l'z}{S}+\frac{\omega^2}{c^2}\psi=0 \quad (50)$$

Additionally by re-writing the term S as:

$$S=\lambda'\theta^2+l'z^2=\lambda'\theta^2(1+\frac{lz^2}{\lambda'\theta^2}) \quad (51)$$

To further simplify the equations, they took the approximation that the spiral growth in the z-direction is much smaller than in the $x-y$ plane thus $\frac{l'z^2}{\lambda'\theta^2}$ converges to zero and can be neglected, in which case, the following terms in equation 50 can be reduced as:

$$\frac{1}{\rho^2}(\frac{\partial\psi}{\partial\theta})\frac{2\lambda'\theta}{S}\approx\frac{1}{\rho^2}(\frac{\partial\psi}{\partial\theta})\frac{2}{\theta} \quad (52)$$

as well as:

$$\frac{\partial\psi}{\partial z}\frac{2l'z}{S}\approx 0 \quad (53)$$

Therefore equation 50 is finally reduced down to:

$$\frac{1}{\rho}\frac{\partial}{\partial\rho}(\rho\frac{\partial\psi}{\partial\rho})+\frac{1}{\rho^2}\frac{\partial^2\psi}{\partial\theta^2}+\frac{\partial^2\psi}{\partial z^2}+\frac{1}{\rho^2}(\frac{\partial\psi}{\partial\theta})\frac{2}{\theta}+\frac{\omega^2}{c^2}\psi=0 \quad (54)$$

Further simplification yields:

$$\frac{\partial^2\psi}{\partial\rho^2}+\frac{1}{\rho^2}\frac{\partial\psi}{\partial\rho}+\frac{1}{\rho^2}\frac{\partial^2\psi}{\partial\theta^2}+\frac{1}{\rho^2}\frac{2}{\theta}\frac{\partial\psi}{\partial\theta}+\frac{\partial^2\psi}{\partial z^2}+\frac{\omega^2}{c^2}\psi=0 \quad (55)$$

By using the method of separation of variables ($\psi = R(\rho)\Theta(\theta)Z(z)$), the equation above is transformed into:

$$\frac{1}{R}\frac{\partial^2 R}{\partial \rho^2} + \frac{1}{\rho R}\frac{\partial R}{\partial \rho} + \frac{1}{\Theta \rho^2}\frac{\partial^2 \Theta}{\partial \theta^2} + \frac{1}{\rho^2}\frac{2}{\Theta\theta}\frac{\partial \Theta}{\partial \theta} + \frac{1}{Z}\frac{\partial^2 Z}{\partial z^2} + \frac{\omega^2}{c^2} = 0 \tag{56}$$

Taking:

$$\frac{1}{Z}\frac{\partial^2 Z}{\partial z^2} = -m^2 \tag{57}$$

yields the Z-component solution $Z = e^{\pm jmz}$. By using the substitution $\frac{\omega^2}{c^2} - m^2 = \gamma^2$, equation 56 can be rewritten as:

$$\frac{1}{R}\frac{\partial^2 R}{\partial \rho^2} + \frac{1}{\rho R}\frac{\partial R}{\partial \rho} + \frac{1}{\Theta \rho^2}\frac{\partial^2 \Theta}{\partial \theta^2} + \frac{1}{\rho^2}\frac{2}{\Theta\theta}\frac{\partial \Theta}{\partial \theta} + \gamma^2 = 0 \tag{58}$$

Multiplying the whole equation by ρ^2 results in:

$$\frac{\rho^2}{R}\frac{\partial^2 R}{\partial \rho^2} + \frac{\rho}{R}\frac{\partial R}{\partial \rho} + \frac{1}{\Theta}\frac{\partial^2 \Theta}{\partial \theta^2} + \frac{2}{\Theta\theta}\frac{\partial \Theta}{\partial \theta} + \gamma^2\rho^2 = 0 \tag{59}$$

Similar to the Z-component, it is assumed that:

$$\frac{1}{\Theta}\frac{\partial^2 \Theta}{\partial \theta^2} + \frac{2}{\Theta\theta}\frac{\partial \Theta}{\partial \theta} = -\alpha^2 \tag{60}$$

Multiplying by Θ results in:

$$\frac{\partial^2 \Theta}{\partial \theta^2} + \frac{2}{\theta}\frac{\partial \Theta}{\partial \theta} + \alpha^2\Theta = 0 \tag{61}$$

By reducing the equation above in general form to standard form, the Θ-component solution can be found as:

$$\Theta = \frac{e^{\pm j\alpha\theta}}{\theta} \tag{62}$$

Finally the radial equation can be simplified to:

$$\frac{\rho^2}{R}\frac{\partial^2 R}{\partial \rho^2} + \frac{\rho}{R}\frac{\partial R}{\partial \rho} + (\gamma^2\rho^2 - \alpha^2) = 0 \tag{63}$$

where if multiplied by R will result in:

$$\rho^2 \frac{\partial^2 R}{\partial \rho^2} + \rho \frac{\partial R}{\partial \rho} + (\gamma^2 \rho^2 - \alpha^2) R = 0 \tag{64}$$

This is a Bessel differential equation, being free of the parameters k and l. Thus the complete solution is given by:

$$\psi(\rho, \theta, z, t) = C J_\alpha(\rho\gamma) \frac{e^{\pm j\alpha\theta}}{\theta} e^{\pm jmz} e^{j\omega t} \tag{65}$$

where C is a constant of integration. Now further boundary conditions can be applied as the impedance is zero at the open end corresponding to $z = z_L$. We know by definition for an irrotational and unsteady flow that:

$$p = -\sigma \frac{\partial \psi}{\partial t} \tag{66}$$

where p is the acoustic pressure and σ the medium density. This equation relates the pressure to the velocity potential in acoustics. We derived before that $Z = \frac{p}{S\dot{u}}$ where $\dot{u}$ is the velocity and therefore one can find:

$$Z = \frac{j\omega\sigma\psi}{S\dot{u}} \tag{67}$$

The fact that $Z = 0$ at the open end requires each one of the independent functions R, Θ, Z to be zero as well. Starting from the Z-component solution, a general solution can be written as:

$$Z = a_m cos(mz) + b_m sin(mz) \tag{68}$$

Taking $a_m = 0$, $Z(z = z_L) = 0$ requires $sin(mz_L) = 0$ thus:

$$m = \frac{n_1 \pi}{z_L} \tag{69}$$

with n_1 as an integer. Similarly for the Θ function, $\Theta(\theta) = 0$ when $sin(\alpha\theta) = 0$ and therefore:

$$\alpha = \frac{n_2 \pi}{\theta} \tag{70}$$

where n_2 is an integer.

From this point onwards, although we do not necessarily agree with the methodology applied in the paper to evaluate the solution constants, we will mention them regardless. They considered their conch shell sample to include a spiral cavity of four turns; corresponding to $\theta = 8\pi$ revolution. Therefore we also have:

$$\alpha = \frac{n_2}{8} \tag{71}$$

Furthermore we have:

$$\frac{\omega}{c} = \sqrt{\gamma^2 + m^2} = \sqrt{\gamma^2 + \frac{n_1^2\pi^2}{z_L^2}} \tag{72}$$

where taking $n = 0$ cancels the frequency growth limiting it to $\frac{\omega}{c} = \gamma$. We know that $J_\alpha(\gamma\rho) = 0$ at $\rho = \rho_L$ corresponding to the open end (mouth). Here the authors selectively choose the parameters p and α so that the zeros of $J_\alpha(\gamma\alpha)$ give harmonic resonance modes. This is based on the conclusion that since the recorded modes are harmonic, thus $p = 4$ and $\alpha = \frac{1}{2}$ based on which we will see the derivation of harmonic modes. However we believe this logic to be artificial as the resonance modes of a system could be non-harmonic, but produce harmonic modes when excited by nonlinear lip-vibration. Nevertheless we continue with their derivations. For the values of p and α given above we have:

$$J_{\frac{1}{2}}(\gamma\rho_L) = \frac{1}{\sqrt{\pi\gamma\rho_L}} sin(\gamma\rho_L) \tag{73}$$

The zeroes occur when $\gamma\rho_L = n_3\pi$ with n_3 being an integer. Thus taking $n_3 = 1$ yields in:

$$\gamma\rho_L = \pi \Leftrightarrow f = \frac{c}{2\rho_L} \tag{74}$$

Therefore the shell's resonance modes being given by $f_n = \frac{nc}{2\rho_L}$.

1.9 Exponential spiral string acoustics

Finally in 2014, Chatterjee and Nayak [13] provided a straightforward study on 1-D wave propagation in an exponential spiral geometry. They considered a spiral in polar coordinates having the

following radius profile:

$$r = r_t e^{\mu\theta} \tag{75}$$

where r_t corresponds to the initial radius (throat radius if considering the conch shell spiral), and μ being the spiral growth factor. μ can also be expressed as a function of the number of spiral turns n (n could also be non-integer):

$$\mu = \frac{1}{2\pi n} ln(\frac{r_m}{r_t}) \tag{76}$$

where r_m is the final end radius (mouth radius in terms of conch shell spiral). The spiral length can also be computed from the relation $L = \int_0^{2\pi n} dl$ where $dl = \sqrt{r^2 + (\frac{dr}{d\theta})^2} d\theta$. For a logarithmic or exponential spiral, the total length will be:

$$L = \sqrt{1 + \frac{1}{\mu^2}}(r_m - r_t) \tag{77}$$

Now the wave equation in 2-D polar coordinates is derived:

$$\frac{\partial^2\psi}{\partial r^2} + \frac{1}{r}\frac{\partial\psi}{\partial r} + \frac{1}{r^2}\frac{\partial^2\psi}{\partial\theta^2} - \frac{1}{c^2}\frac{\partial^2\psi}{\partial t^2} = 0 \tag{78}$$

since r and θ are directly related, the θ derivatives can be substituted by the r derivatives using:

$$\frac{\partial^2\psi}{\partial\theta^2} = \mu^2 r^2 \frac{\partial^2\psi}{\partial r^2} + \mu^2 r \frac{\partial\psi}{\partial r} \tag{79}$$

Using Helmholtz time-independent version of the wave equation and using the substitution above, the radial part of the equation can be written as:

$$r^2 \frac{d^2\psi(r)}{dr^2} + r\frac{d\psi(r)}{dr} + k^2 r^2 \psi(r) = 0 \tag{80}$$

where $k^2 = \frac{\omega^2}{c^2(1+\mu^2)}$. It can be noted that the partial derivatives are replaced by direct derivatives as the radial component of the solution is considered.

Comparing the new expression for the wave number k and comparing it to the classic definition of $k = \frac{\omega}{c}$, we can see that the extra term $\frac{1}{1+\mu^2}$ scales the frequencies. The dispersion relation thus

depends on the geometry of the spiral (i.e. the spiral's growth factor μ). It was previously noted that μ and n have an inverse relation, thus the higher n is, the closer the new dispersion relation gets to the quantity $\frac{\omega}{c}$.

Equation 80 is a Bessel differential equation and thus the solution is given in terms of the Bessel and Neumann functions as:

$$\psi(r) = AJ_0(kr) + BN_0(kr) \tag{81}$$

where J_0 and N_0 are the Bessel and Neumann functions of order 0, respectively. It is also worth noting that this case is similar to the derivation of the wave equation in polar coordinates, where in both cases a Bessel differential equation is to be solved.

To evaluate the constants A and B, the authors considered two different boundary conditions.

The first being a spiral string fixed at both of its ends, we have $\psi(r = r_t) = \psi(r = r_m) = 0$, therefore the solution will take the form:

$$\psi = \sum_{n=1} C_n[cos\delta J_0(k_n r) + sin\delta N_0(k_n r)]cos(\omega_n t) \tag{82}$$

where δ is taken such that the boundary condition at $r = r_m$ is satisfied, leading to:

$$tan\delta = -\frac{J_0(k_n r_m)}{N_0(k_n r_m)} \tag{83}$$

To find the values of k_n which satisfy the equation above, the following equation must be solved:

$$cos\delta J_0(k_n r_t) + sin\delta N_0(k_n r_t) = 0 \tag{84}$$

The authors numerically computed 5 values of k_n for $n = 1, 2, 3, 4, 5$ with a fixed value of $r_m = 1$ and few values of $r_t = 0.1, 0.2, 0.3, 0.4, 0.5$.

The next boundary condition is when there exists an oscillation at the input of the string ($r = r_t$) but rigidly fixed at the end ($r = r_m$). It was taken that $\psi(r = r_t, t) = Fcos(\Omega t)$ and $\psi(r = r_m, t) = 0$. As previously explained, the solution is a combination of Bessel and Neumann functions:

$$\psi(r) = C[cos\delta J_0(kr) + sin\delta N_0(kr)]cos(\Omega t) \tag{85}$$

where C and δ must be evaluated. From the B.C. at $r = r_m$ it is obtained:

$$tan\delta = -\frac{J_0(kr_m)}{N_0(kr_m)} \tag{86}$$

And from the B.C. at $r = r_t$ it is found that:

$$C = \frac{F}{cos\delta J_0(kr_t) + sin\delta N_0(kr_t)} \tag{87}$$

where the authors claim that C cannot be evaluated at resonance and the solution cannot be found theoretically.

In this chapter we reviewed key acoustic theories on cylindrical, conical and exponential ducts. We also reviewed four different acoustic models for the conch shell: i) Approximation by a straight duct ii) The conch shell modelled as a conical spiral cavity iii) A model based on Webster's horn equation and iv) The shell's cavity modelled as an exponential spiral string. In the next chapter we will present our experiments on the conch shell where we geometrically modelled the shell's cavity using X-ray scans and performed spectrum analysis in different excitation cases.

Chapter 2

Experiments

We saw from the early studies by Bhat [6] [7] that by using X-ray tomography scans one can geometrically model the inner spiral cavity of a conch shell. We attempted to re-verify using our own sample, which is of the "Turbinella Pyrum" family of shells. Our shell had the throat cut in order to facilitate playing the shell, and was of rigid material suitable for wave propagation inside. In the first section of this chapter, we will provide details on how the geometry of the spiral cavity was deduced from the X-ray scans, as well as the presence of Fibonacci patterns within the cavity. It is worth mentioning that there are a few advanced mathematical models for the conch shell geometry, such as the following parametrization by von Seggern [14]:

$$x = [a(1 - \frac{\nu}{2\pi})(1 + cosu) + c]cos(n\nu) \tag{88}$$

$$y = [a(1 - \frac{\nu}{2\pi})(1 + cosu) + c]sin(n\nu) \tag{89}$$

$$z = \frac{b\nu}{2\pi} + asinu(1 - \frac{\nu}{2\pi}) \tag{90}$$

where parameters $u, \nu \in [0, 2\pi]$, a, b, c as arbitrary constants and n an integer. However as it is clear, such geometrical models are not useful for acoustic applications as they overcomplicate mathematical derivations with no workarounds.

Figure 2.1: The Turbinella Pyrum conch shell sample used throughout the thesis.

2.1 Geometrical modelling of the inner spiral cavity of a conch shell

The X-ray scans are provided from 3 different points of view: Axial, Coronal and Sagittal views. Figures 2 to 4 display an X-ray screenshot (211th shot) of the shell from all three views. The axial scan is not suitable to deduce the spiral geometry of the shell and in essence, useless in terms of modelling the inner cavity as it provides little to no information. However, the scan in sagittal view has all the elements required to approximate the inner cavity as a wrapped version of a conical or exponential straight tube.

In Figure 2.2, the spiral cavity takes a π turn at each step. Therefore the angular distance between the consecutive cavities indicated in the scan is equal to π. Thus we know that the spiral takes a total of 6π turns. Now we need to measure the spiral radius at each turn, and thus approximate a profile to it. It is natural to select the measurement points as in figure 2.5, and measure their orthogonal distance to the axis of revolution that passes through the shell (or cuts the shell in two equal halves). The measurements were done in the image processing software "Fiji", and the scale was deduced from the X-ray's own pre-defined scale indicated at the bottom of the scans. However in order to complete the 3-D profile of the spiral cavity, we also need the relative height of the spiral at each turn. The measurements are presented in table 2.1. In order to arrive at a profile for the

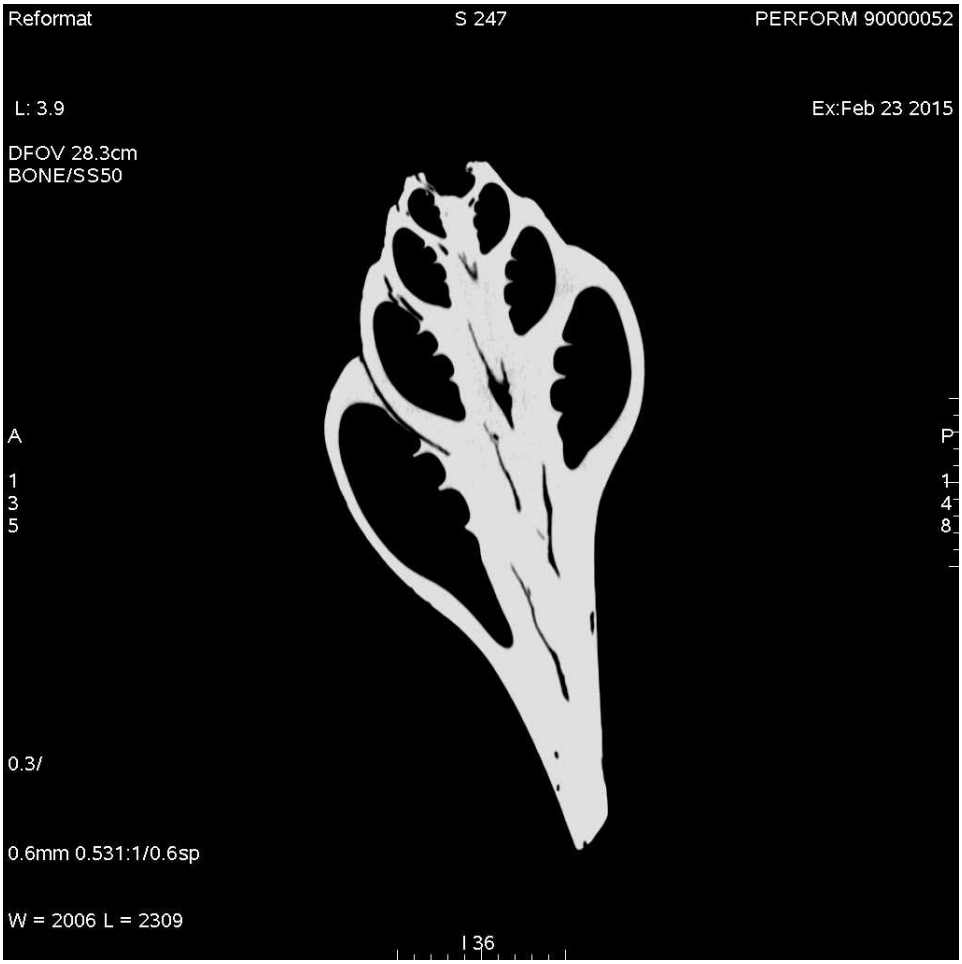

Figure 2.2: Sagittal view.

Angle	Radius 1	Height	Radius 2-R	Radius 2-L	Radius 3-T	Radius 3-B
0	10.57mm	58.22mm	2.69mm	4.46mm	8.09mm	8.01mm
π	12.97mm	55.31mm	3.61mm	6.24mm	10.62mm	10.33mm
2π	17.26mm	48.37mm	3.84mm	6.70mm	15.31mm	11.74mm
3π	21.69mm	41.07mm	6.69mm	9.04mm	16.11mm	16.68mm
4π	27.67mm	27.60mm	7.32mm	10.18mm	21.75mm	20.15mm
5π	35.48mm	19.50mm	8.68mm	14.30mm	28mm	27.11mm
6π	43.20mm	0mm	12.42mm	14.65mm	36.50mm	49.59mm

Table 2.1: Radius 1 corresponds to the spiral's radius at each π turn. Height corresponds to the relative spiral turn at each turn. Radius 2-R corresponds to the minor axis's right side radius of the cross-section, where Radius 2-L corresponds to the axis's left side radius of the cross-section. Radius 3-T and 3-B correspond to the major axis's top and bottom radius of the cross-section, respectively.

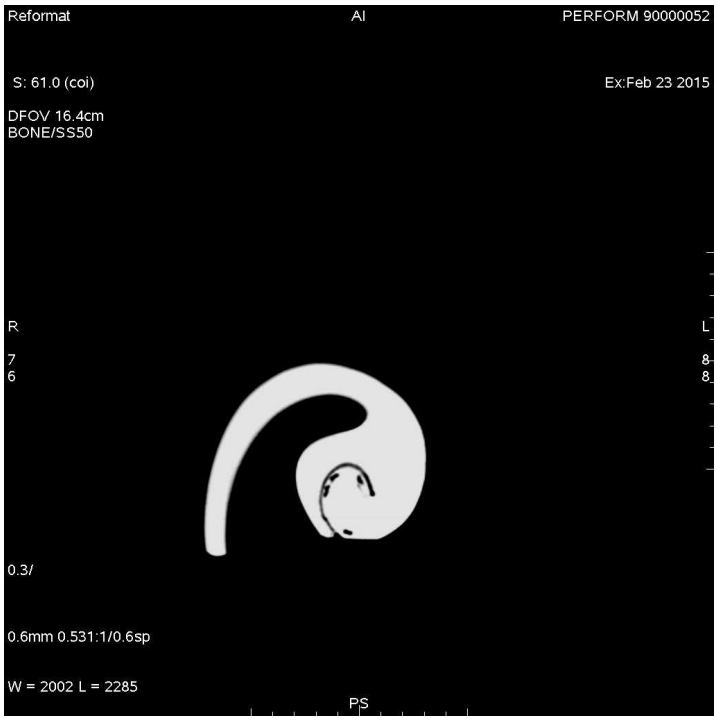

Figure 2.3: Axial view.

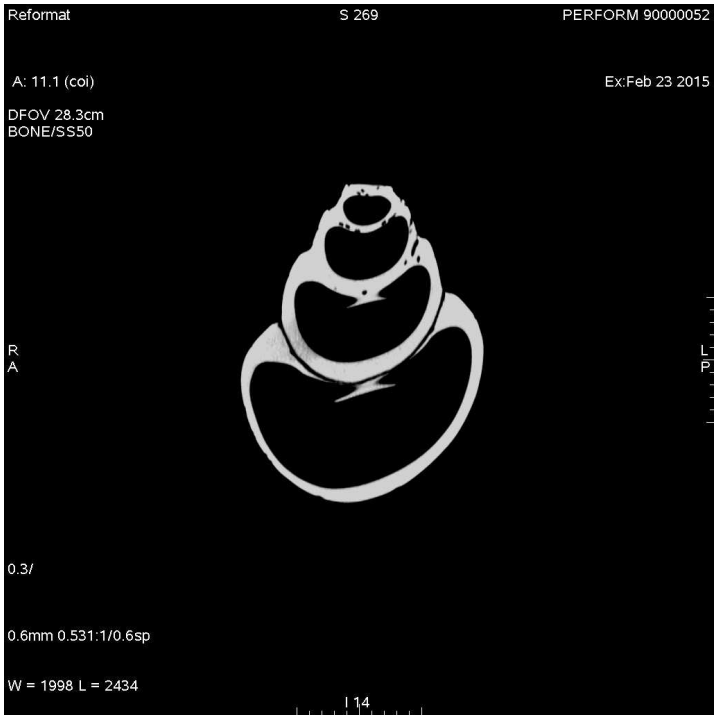

Figure 2.4: Coronal view.

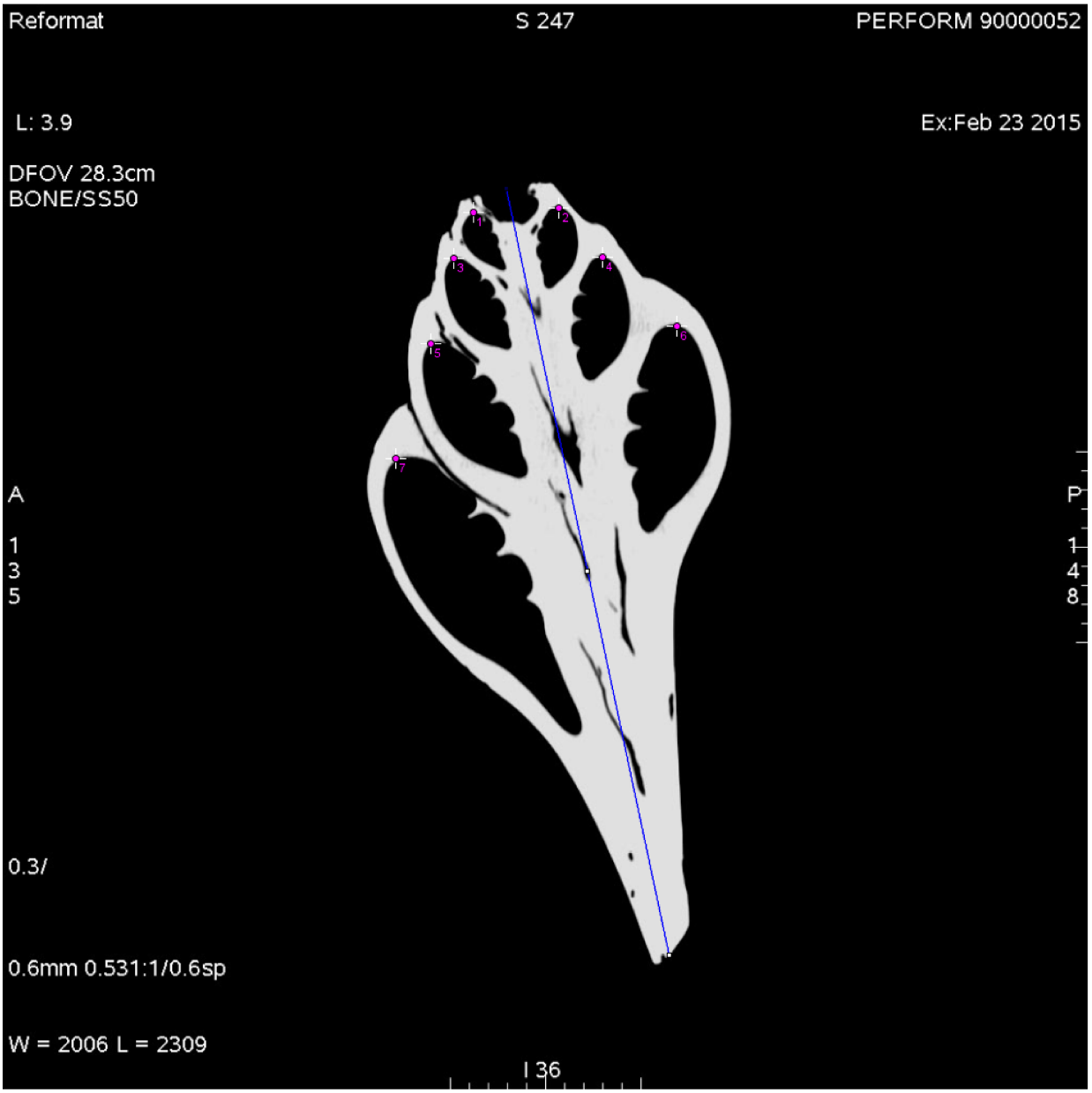

Figure 2.5: The radius at each π turn is determined by the orthogonal distance between the purple points and the blue axis of revolution.

spiral cavity, we approximated piecewise portions of the spiral using conical spirals of form $\rho = \alpha\theta$ where the parameter α may vary based on the portion of spiral in consideration. For our sample, we came up with the following profile: For $\theta_1 = [0, 4\pi]$, $\rho_1 = 0.125\theta_1 + 1.05$ and for $\theta_2 = [4\pi, 6\pi]$, $\rho_2 = 0.225\theta_2$. A fit of these conical spirals to the measured data on a 2-D polar plane is shown in the figure 2.6.

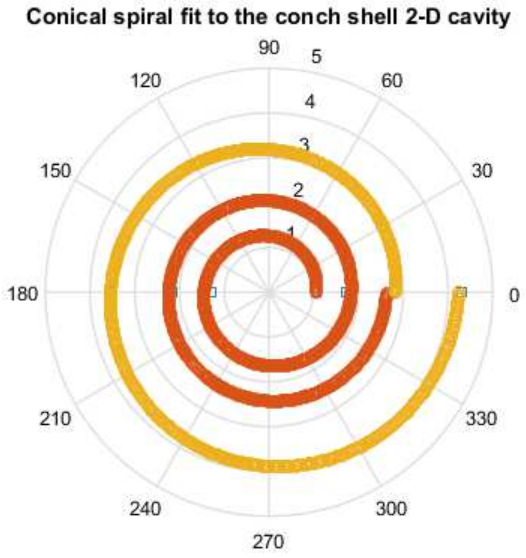

Figure 2.6: Piecewise spiral fit to the measured radii on 2-D polar plane.

Furthermore, the radius-height profile is also plotted, where a second order polynomial fit is applied. We approximated $z(\rho) = p_1\rho^2 + p_2\rho + p_3$ where $(p_1, p_2, p_3) = (-0.079, -1.331, 7.342)$ with a fit goodness of R-square = 0.9922. Using equation 36, we found the total spiral length to be approximately equal to $55cm$. In addition, the major and minor axes radii profiles are also plotted which show the profile of the unwrapped spiral cavity.

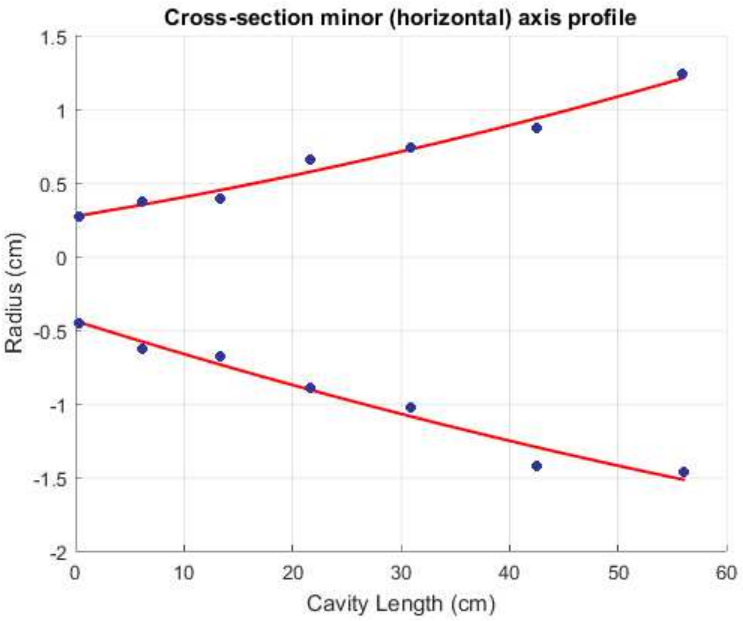

Figure 2.7: Minor radius-cavity length profile of the conch shell.

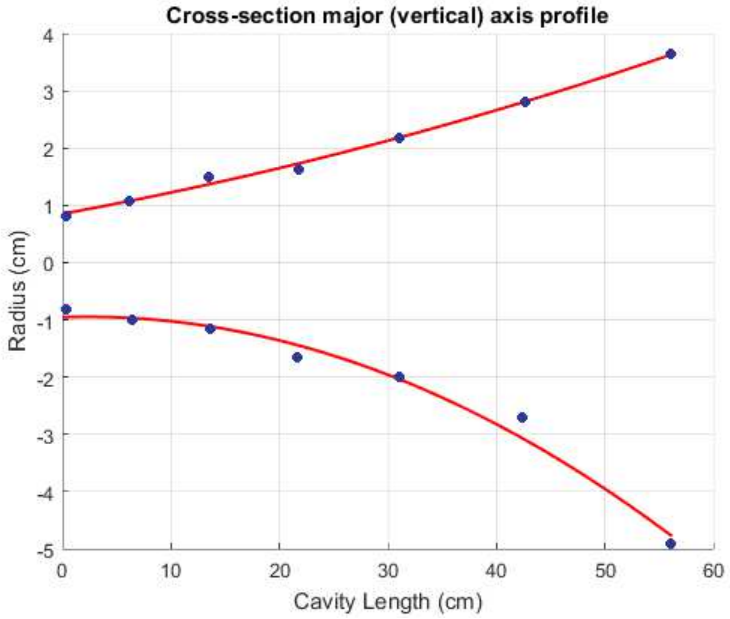

Figure 2.8: Major radius-cavity length profile of the conch shell.

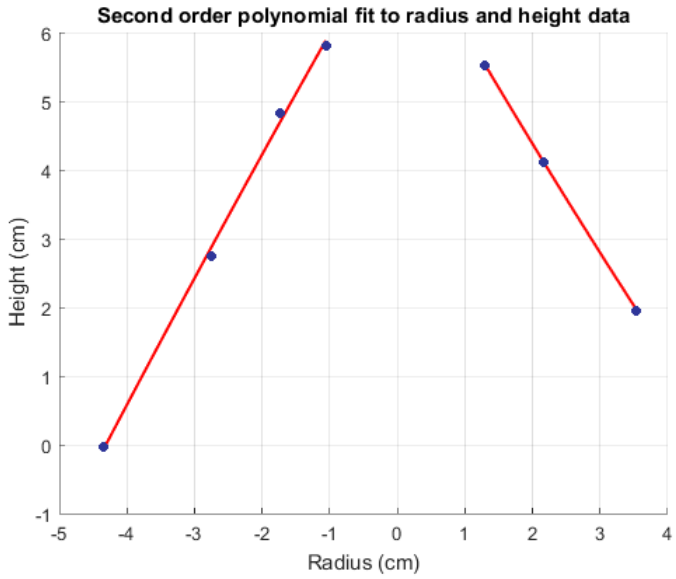

Figure 2.9: Height-radius profile of the conch shell. The negative radii values only indicate the shell's actual geometry. The second order polynomial height-radius fit is obtained using the radii absolute values.

As we see from figures 2.7 and 2.8, there is no sudden appearance of a flare in the cross-section profile and thus it is safe to assume that the standing wave is actually reflected at the end of the cavity, and not before it. This also means that the acoustical length is taken to be approximately equal to the physical length of $55cm$. To support this assumption, we also did a spectrum analysis of the resonance modes.

2.2 Spectrum Analysis

We excited the conch shell in 3 different ways: (i). Loudspeaker sine sweep (ii). Electro-Pneumatic Transducer and (iii). Lip-vibration. We also attempted a square wave sweep measurement which contains harmonics, however due to the fact that the shell's response gave no useful information, the results on that are not included. The MATLAB codes corresponding to the full geometrical modelling of the shell are provided in Appendix A.

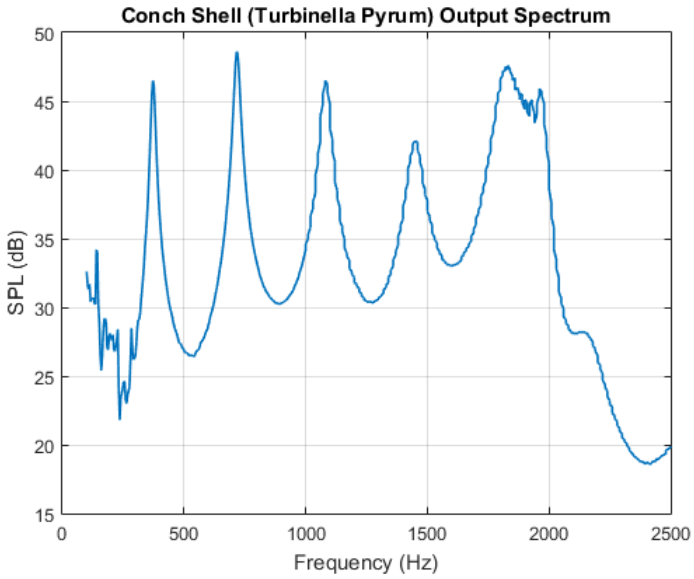

Figure 2.10: The Turbinella Pyrum resonance modes at 372, 716, 1080, 1450 and 1830 Hz

2.2.1 Loudspeaker Sine Sweep Measurement

The sine sweep tests were done by attaching a small loudspeaker to the throat of the conch shell. The settings for the sine sweep were a frequency span of $100 - 2000Hz$ and a time duration of 1 second. As it can be seen from figure 2.10, the resonance modes are approximately harmonics of the fundamental frequency of $372Hz$, however, shifted and with margins of error due to the fact that the spiral cavity geometry is not perfect. But the spectrum does indicate that the spiral cavity may be a wrapped conical tube around a central stem. [1]

2.2.2 Electro-Pneumatic Transducer (EPT)

In this setup the conch shell was excited by an Electro-pneumatic transducer, operating at $52Hz$. The motivation behind this measurement was to see how the shell would respond to a different type of excitation and how closely the EPT can simulate the reed mechanics of lip-vibration. The output spectrum displayed $3k + 4$ multiples of the driver frequency ($52Hz$) and provided a clear pattern. However not much more information can be deduced due to the non-linear nature of the EPT excitation.

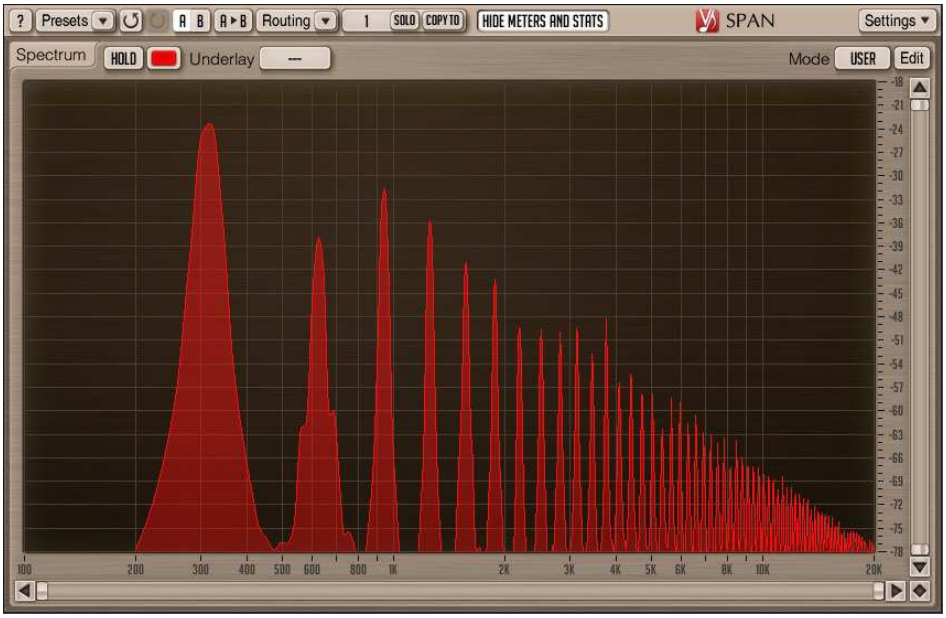

Figure 2.11: Frequency spectrum for lip-vibration, resonance modes at 372, 716, 1080, 1450 and $1830Hz$.

2.2.3 Lip-vibration

When we played the shell with lip excitation, clear harmonic resonance modes were present with the first 5 modes being: 315, 626, 944, $1.26K$ and $1.57K$ Hz. We previously approximated the conch shell's acoustics to those of a $55cm$ conical tube. If the conical tube's output to input diameter ratio is small enough (which is the case as seen from the radii profiles), the resonance modes of a $55cm$ conical tube will derive from $f_n = \frac{nc}{2L}$ where $L = 55cm$. Therefore the first five estimated frequencies will be: 312, 624, 936, 1.25K and 1.56K Hz. It can be seen from table 2.2 that there is strong correspondance between the estimated frequencies and the resonance modes of the lip-excited shell. This further supports the assumption that a conch shell's spiral cavity acoustics may be approximated by an equivalent conical tube with the appropriate dimensions.

2.2.4 Input Impedance

An important characteristic of musical instruments are their input impedances. In chapter 1, we saw how the derivation of input impedances of frusta of various geometries could lead to important

Loudspeaker	EPT	Lip-vibration	Estimation
372	52	315	312
716	208	626	624
1.08K	364	944	936
1.45K	520	1.26K	1.25K
1.83K	676	1.57K	1.56K

Table 2.2: Resonance modes of the Turbinella Pyrum conch shell in different excitation cases (in Hertz). The estimated resonance frequencies correspond to the theoretical resonance modes of an equivalent conical tube to the shell's spiral cavity.

results such as the resonance modes and the impulse response of the system. Due to the irregular geometry of the conch shell, a theoretical derivation of its input impedance is difficult. However it can be experimentally measured using an input impedance measuring device. The one used in our case applied a basic sine sweep up to $4000Hz$ and the result is displayed in figure2.12. The first five resonance peaks are $313, 623, 972, 1339, 1665Hz$ which compared with the estimated resonance modes and those recorded from lip-vibration (table 2.2). There is good enough correspondence, although the resonance harmonicity starts getting weaker after the first two modes.

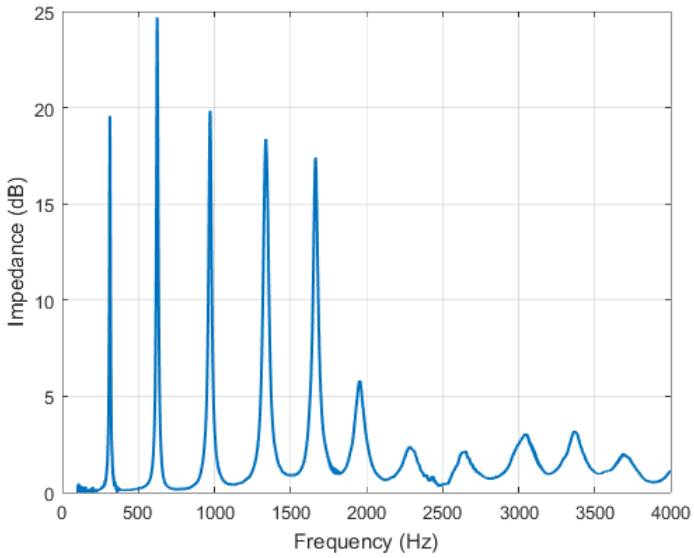

Figure 2.12: Input impedance of the conch shell - resonance modes at $313, 623, 972, 1339, 1665Hz$

It is also worth mentioning that since we measured the input impedance, knowing the maximum frequency ($4000Hz$), the frequency-step ($df = 0.2Hz$) and consequently the number of frequency evaluation points, we can also compute the impulse response of the shell based on the inverse fast Fourier transform (IFFT) of the input impedance. The impulse response shows how the shell output reacts to a very short input signal (impulse), in other words the shell's time-dependent reaction characterizing the shell's dynamic behavior.

We also want to note that we tried approximating the input impedance of the shell by computing the input impedance of several concatenated conical/cylindrical tubes via digital waveguide modelling. However the computed input impedance did not match the measured impedance which is attributable to the irregularity of the shell's geometry. In order to maintain the scope of the study focused, we will omit getting into the details of digital waveguide modelling of musical bores.

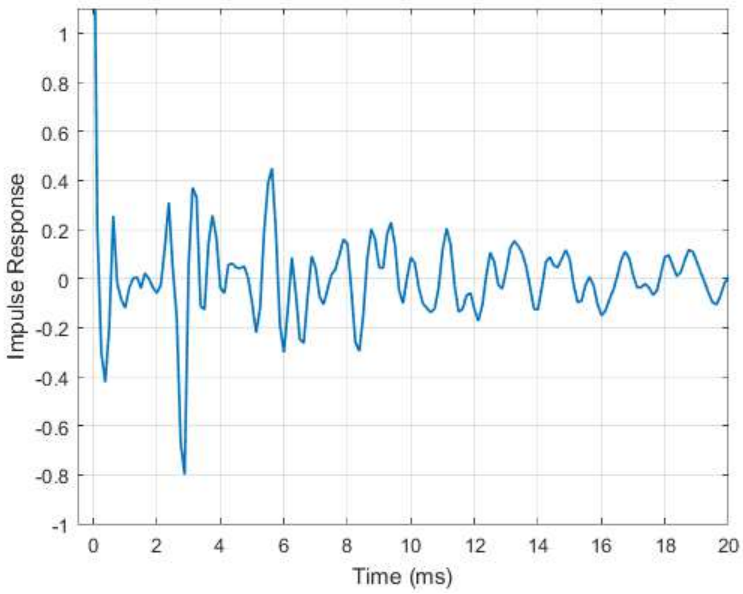

Figure 2.13: Impulse response of the conch shell.

2.3 Directivity-Pattern

Directivity measurements of the loudspeaker and EPT-driven conch shell in both horizontal and vertical alignments inside a semi-anechoic chamber were carried out. The chamber dimensions

were 164" x 120" x 96" (Length x Width x Height) with 3 panels wide and 4 panels long, where standard acoustic foam wedges of approximately 10 cm thickness was used. The wall and ceiling panels were 40" x 96" and 40" x 116" large, respectively. The shell was positioned at the center of the room, mounted on a tripod with the loudspeaker attached to the shell's throat. The recording microphone was placed 1.35 m in front of the shell's mouth to capture the output. The loudspeaker was driven at a frequency near the shell's cavity resonance (approximately 300Hz) and the shell was rotated at 60° angular increments about both its longitudinal and transverse axes in order to obtain the 2-D 360° directivity pattern (in both Horizontal and Vertical alignments of the shell). A similar setup was used for the EPT driver. Based on the recorded magnitudes, the conch shell sample proved to be an omni-directional (direction-independent) sound radiator at frequencies near its cavity resonance. The horizontal or vertical alignments made no considerable difference.

Degree	LS-H	LS-V	EPT-H	EPT-V
0	73.7	73.9	55.1	55.1
60	73.1	72.8	53.4	53.5
120	73.1	72.2	53.0	52.5
180	73.6	72.8	53.9	53.0
240	74.6	73.6	55.2	54.3
300	74.5	73.6	53.9	53.2

Table 2.3: The captured output magnitude (in dB) for the loudspeaker (LS) and EPT excitations at 310 Hz in both horizontal (H) and vertical (V) alignments.

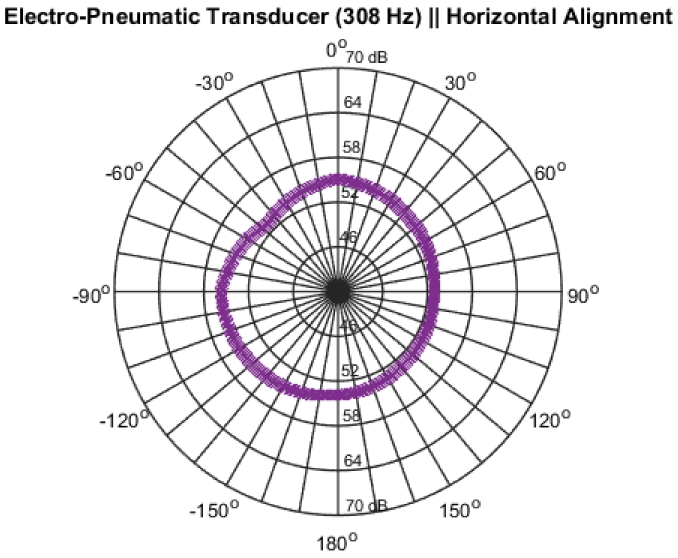

Figure 2.14: Directivity diagram of the EPT driven shell at $308 Hz$ in horizontal alignment. The radiation pattern displays uniformity and hence omni-directional.

2.4 Fibonacci Pattern in cavity structure

As mentioned previously, Rath and Naik [8] studied the geometry of two different types of shells and found the clear presence Fibonacci patterns. We also verified that our conch shell sample contains Fibonacci patterns with proper selection points. The distance between the consecutive green points and pink points in figure 2.15 follow the Fibonacci pattern. We also tried overlapping the conch shell spiral from axial point of view on a golden spiral, however, they did not match.

Distance between points	Green Points	Pink Points
1 & 2	23 mm	12 mm
3 & 4	40 mm	22 mm
5 & 6	63 mm	34 mm

Table 2.4: The Fibonacci pattern is clearly present with the correct selection of parameters, as originally demonstrated by Rath and Naik.

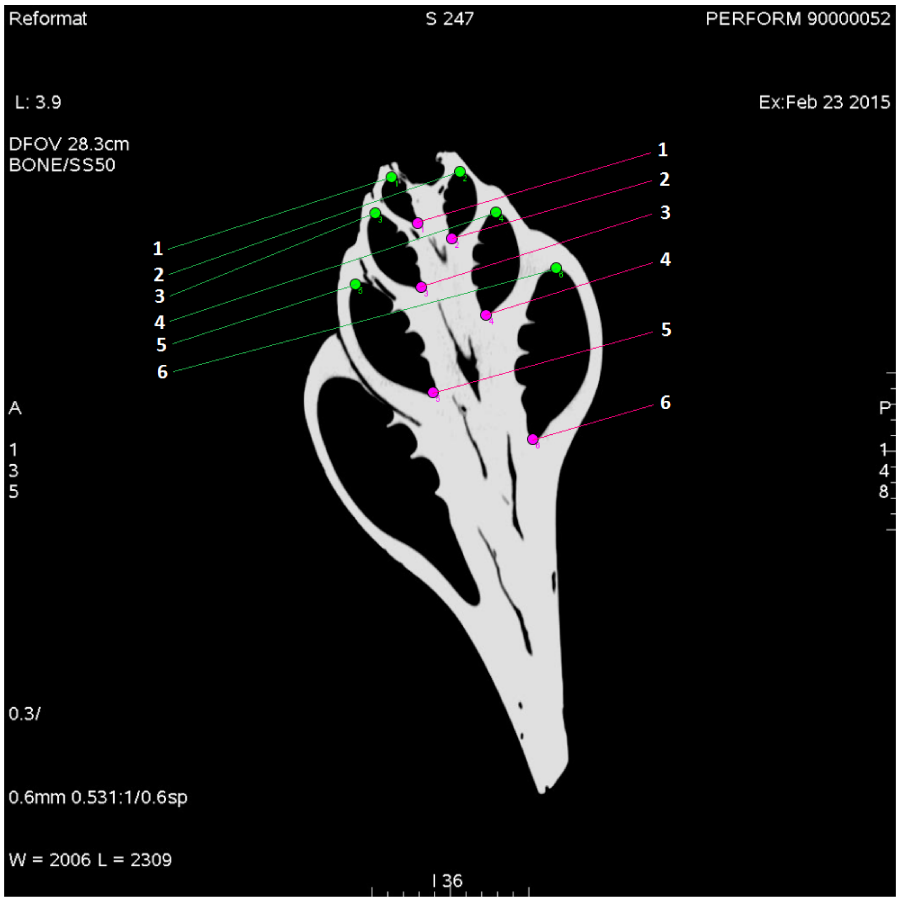

Figure 2.15: Axial view of the shell X-ray scan with selection points, indicating the presence of Fibonacci pattern in the cavity growth structure.

In this chapter we provided a geometrical model of the shell's cavity using X-ray scans, where we showed that it is essentially a wrapped conical tube in terms of acoustic properties. We also performed spectrum analysis in three excitation cases: i) Lip-vibration ii) Loudspeaker and iii) Electro-pneumatic transducer. Directivity measurements were also done in a semi-anechoic chamber, using loudspeaker and Electro-pneumatic transducer excitations. Finally, we displayed the presence of the Fibonacci pattern in the shell's cavity growth with the proper selection points. In the next chapter we focus on the time-domain behaviour of wave propagation in spiral geometries using numerical analysis, as well as theoretical derivations of wave propagation in an exponential spiral tube based on Webster's horn equation.

Chapter 3

Theory and Numerical Analysis

3.1 Wave propagation analysis in spiral geometries

In this section we take a look at wave propagation in spiral geometries from a more numerical point of view which seems to be lacking in the studies done so far. We start from a simple case of 3-D time-independent wave propagation inside an exponential spiral string. The core difference between this case and the one covered by Nayak [13] is that here we consider the presence of an extra variable height z, where Nayak derived the equations in 2-D polar coordinates, not considering the effect of height in wave propagation.

We still have a spiral of profile $r = r_t e^{\mu\theta}$ where r_t is the initial radius and μ the spiral growth factor. Additionally, we consider the spiral height profile to be of form $z = \alpha r$ where α is basically a tapering parameter. The spiral length is determined from:

$$L = \int dl = \int \sqrt{r^2 + (\frac{dr}{d\theta})^2 + (\frac{dz}{d\theta})^2} d\theta \tag{91}$$

We have $\frac{dr}{d\theta} = r_t \mu e^{\mu\theta}$ and $\frac{dz}{d\theta} = \alpha r_t \mu e^{\mu\theta}$. Therefore it can be easily found that:

$$L = \sqrt{1 + \alpha^2 + \frac{1}{\mu^2}}(r_m - r_t) \tag{92}$$

where r_m is the final radius. We see that the spiral length and the taper parameter α are directly proportionate.

We now attempt to derive the time-independent wave equation in 3-D cylindrical coordinates for our given geometry:

$$\frac{\partial^2\psi}{\partial r^2} + \frac{1}{r}\frac{\partial\psi}{\partial r} + \frac{1}{r^2}\frac{\partial^2\psi}{\partial\theta^2} + \frac{\partial^2\psi}{\partial z^2} + k^2\psi = 0 \tag{93}$$

Since θ and z are both directly related to the radius r, we have $\frac{\partial^2\psi}{\partial\theta^2} = \mu^2 r^2\frac{\partial^2\psi}{\partial r^2} + \mu^2 r\frac{\partial\psi}{\partial r}$ and $\frac{\partial^2\psi}{\partial z^2} = \frac{1}{\mu^2 z^2}\frac{\partial^2\psi}{\partial z^2} - \frac{1}{\mu z^2}\frac{\partial\psi}{\partial\theta}$. After substituting the two terms into equation 90 and upon simplifying, we obtain (radial part of equation):

$$\frac{d^2\psi}{dr^2} + \frac{\lambda}{r}\frac{d\psi}{dr} + \kappa^2\psi = 0 \tag{94}$$

where $\kappa^2 = \frac{k^2}{1+\mu^2+\frac{1}{\alpha^2}}$ with $k = \frac{\omega}{c}$ and $\lambda = \frac{1+\mu^2}{1+\mu^2+\frac{1}{\alpha^2}}$. Equation 91 can be solved based on the transformed version of the Bessel differential equation given by Bowman (1958), where for an equation of the type:

$$x^2\frac{d^2y}{dx^2} + (2p+1)x\frac{dy}{dx} + (a^2x^{2r} + \beta^2)y = 0 \tag{95}$$

The solution is given by:

$$y = x^{-p}[C_1 J_{\frac{q}{r}}(\frac{a}{r}x^r) + C_2 Y_{\frac{q}{r}}(\frac{a}{r}x^r)] \tag{96}$$

where $q = \sqrt{p^2 - \beta^2}$. Therefore the solution for equation 91 is:

$$\psi = r^{\frac{1-\lambda}{2}}[C_1 J_p(\kappa) + C_2 Y_p(\kappa r)] \tag{97}$$

In order to evaluate the constants C_1 and C_2 we can use the boundary conditions of $\psi(r = r_t) = 1$ a constant input to the string, and $\psi(r = r_m) = 0$, the string being fixed at the end. In that case we have:

$$C_2 = \frac{1}{r_t^{-p}[Y_p(kr_t) - \frac{Y_p(kr_m)J_p(kr_t)}{J_p(kr_m)}]} \tag{98}$$

$$C_1 = -C_2\frac{Y_p(kr_m)}{J_p(kr_m)} \tag{99}$$

In figure 3.1 we have plotted the solution over 100 space-steps.

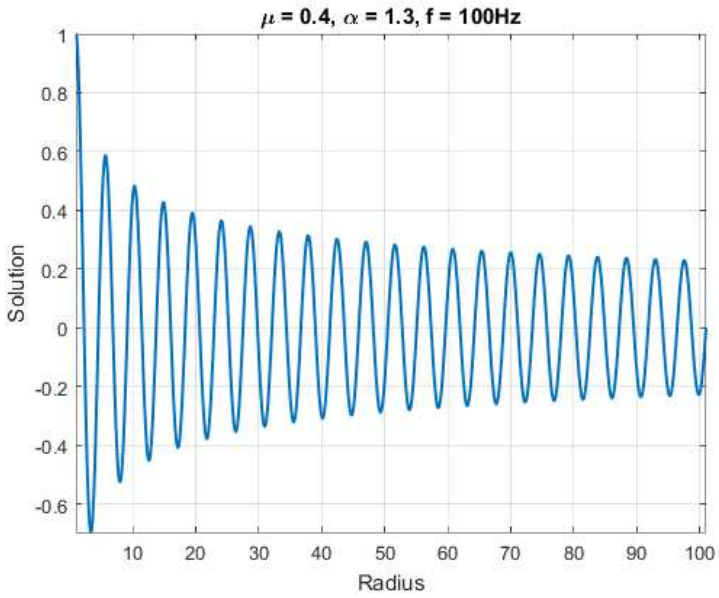

Figure 3.1: Solution to equation 94 for $\mu = 0.4$, $\alpha = 1.3$ and $f = 100Hz$

We also plot the profile of the term $(\frac{\kappa}{k})^2$ as a function of the number of spiral turns n (μ and n being related by equation 76):

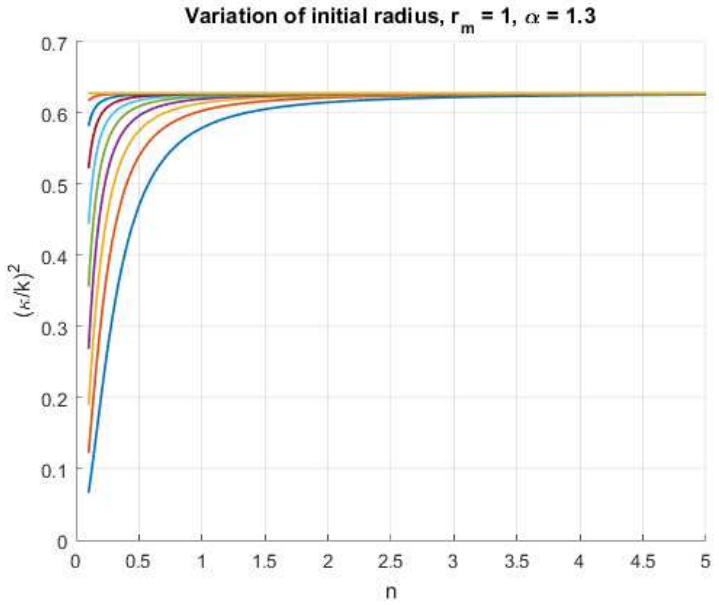

Figure 3.2: Profile of the ratio $(\frac{\kappa}{k})^2$ in terms of spiral turns n, for different initial radii values r_t.

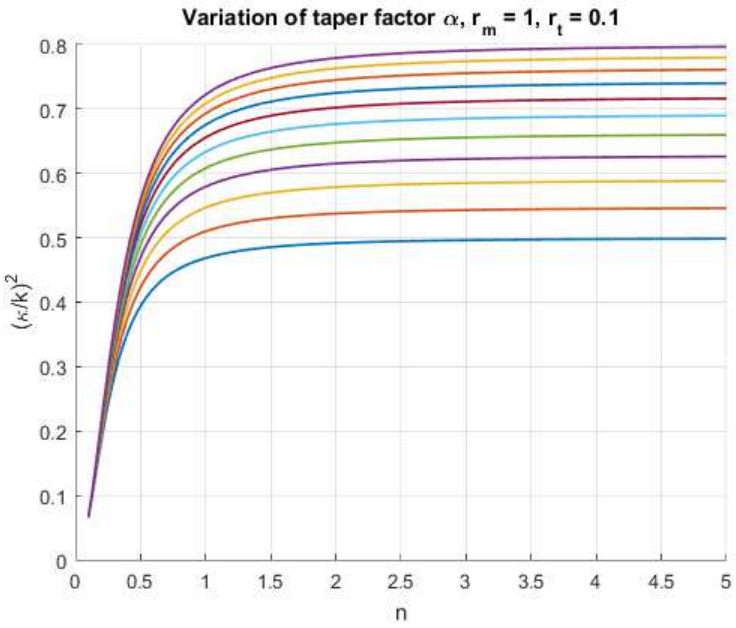

Figure 3.3: Profile of the ratio $(\frac{\kappa}{k})^2$ in terms of spiral turns n, with the varying parameter α.

The MATLAB codes used in this section are provided in Appendix A.

3.2 Time-dependent behavior of wave propagation in a spiral geometry

Until now, most of the theoretical derivations were based on the fact that a lip-excited shell produces harmonic resonance modes. The theories were either adjusted or derived in a way to satisfy that condition. However due to the non-linearity of the lips reed mechanics, such approach may not be optimal although correlates well with experiments and existing acoustic theories. Another deficiency is the fact that the time-dependent behavior of the wave propagation inside the shell was mostly neglected since the wave equation was derived in its time-independent form (Helmholtz equation). We attempted to numerically simulate the time-domain behavior of wave propagation in a conch shell using finite difference techniques. We also extended the study case to 3-D profiling of a spiral geometry.

3.2.1 Exponential spiral string

We define an exponential spiral geometry of $\rho = \rho_t e^{\mu\theta}$ with a height profile $z = \alpha\rho$ which we have dealt with earlier. We will derive the wave equation in cylindrical coordinates, in adding a damping term $\nu\frac{\partial\psi}{\partial t}$:

$$c^2\{\frac{1}{\rho}\frac{\partial\psi}{\partial\rho} + \frac{\partial^2\psi}{\partial\rho^2} + \frac{1}{\rho^2}\frac{\partial^2\psi}{\partial\theta^2} + \frac{\partial^2\psi}{\partial z^2}\} = \frac{\partial^2\psi}{\partial t^2} + \nu\frac{\partial\psi}{\partial t} \tag{100}$$

Replacing the θ and z derivatives in terms of ρ derivatives simplifying the equation results in:

$$\frac{\partial^2\psi}{\partial\rho^2} + \frac{\lambda}{\rho}\frac{\partial\psi}{\partial\rho} - \zeta\frac{\partial^2\psi}{\partial t^2} - \eta\frac{\partial\psi}{\partial t} = 0 \tag{101}$$

where:

$$\lambda = \frac{1+\mu^2}{1+\mu^2+\frac{1}{\alpha^2}} \tag{102}$$

$$\zeta = \frac{1}{c^2(1+\mu^2+\frac{1}{\alpha^2})} \tag{103}$$

$$\eta = \frac{\nu}{c^2(1+\mu^2+\frac{1}{\alpha^2})} \tag{104}$$

In order to display the wave propagation in both time and space domains, we attempt to solve the equation numerically. Since the equation is hyperbolic, naturally an explicit finite difference scheme centered in time and space is applied, also known as the three-point central difference scheme [15]. Defining the space the time meshes as $\rho_n = n\Delta\rho$ and $t_k = k\Delta t$, respectively with n and k integers and $d\rho$ and dt the space and time steps, respectively. Therefore the numerical scheme is defined as:

$$\frac{\partial\psi}{\partial\rho} \approx \frac{\psi^k_{n+1} - \psi^k_{n-1}}{2\Delta\rho} \qquad \frac{\partial^2\psi}{\partial\rho^2} \approx \frac{\psi^k_{n+1} - 2\psi^k_n + \psi^k_{n-1}}{\Delta\rho^2} \tag{105}$$

$$\frac{\partial\psi}{\partial t} \approx \frac{\psi^{k+1}_n - \psi^{k-1}_n}{2\Delta t} \qquad \frac{\partial^2\psi}{\partial t^2} \approx \frac{\psi^{k+1}_n - 2\psi^k_n + \psi^{k-1}_n}{\Delta t^2} \tag{106}$$

Substituting these terms into equation 98 and after simplification, we obtain:

$$\psi^{k+1}_n = -(c_1 + \frac{c_2}{n})\psi^k_{n+1} + 2(c_1 - c_3)\psi^k_n + (\frac{c_2}{n} - c_1)\psi^k_{n-1} + (c_3 - c_4)\psi^{k-1}_n \tag{107}$$

$$c_1 = (-\Delta\rho^2(\frac{\zeta}{\Delta t^2} + \frac{\eta}{2\Delta t}))^{-1} \qquad c_2 = \frac{-\lambda}{2\Delta\rho^2(\frac{\zeta}{\Delta t^2} + \frac{\eta}{2\Delta t})} \tag{108}$$

$$c_3 = \frac{-\zeta}{\Delta t^2(\frac{\zeta}{\Delta t^2} + \frac{\eta}{2\Delta t})} \qquad c_4 = \frac{-\eta}{2\Delta t(\frac{\zeta}{\Delta t^2} + \frac{\eta}{2\Delta t})} \tag{109}$$

The solution at time step $k = 0$ requires the value of ψ_n^{-1} which physically does not exist (since time cannot be negative) however mathematically, we can approximate the quantity by using the initial velocity condition $g(\rho)$ as:

$$\psi_n^{-1} \approx \psi_n^1 - 2\Delta t g(\rho_n) \tag{110}$$

Therefore the value of ψ_n^1 can be expressed independent of the term ψ_n^{-1} as:

$$\psi_n^1 = -\frac{c_1 + \frac{c_2}{n}}{1 - c_3 + c_4}\psi_{n+1}^0 + 2\frac{c_1 - c_3}{1 - c_3 + c_4}\psi_n^0 + \frac{\frac{c_2}{n} - c_1}{1 - c_3 + c_4}\psi_{n-1}^0 - 2\Delta t\frac{c_3 - c_4}{1 - c_3 + c_4}g(\rho_n) \tag{111}$$

We took $\rho_n = [0, 1, 2, ..., L]d\rho$ and $t_k = [0, 1, 2, ..., T]dt$ where $L = 10^2$, $T = 10^4$, $d\rho = 1$ and $dt = 10^{-3}$. The wave velocity was taken as the standard velocity at room temperature as $347\frac{m}{s}$ and an initial velocity condition of $g = 0$.

For the time domain representation, we chose boundary conditions of $\psi(\rho = 0, t) = sin(2\pi ft)$ where $f = 50Hz$ the input sine frequency, and $\psi(r = L, t) = 0$ as the string is fixed at the end. We saw a reflecting wave from $\rho = 0$ and $\rho = L$ travelling back and forth.

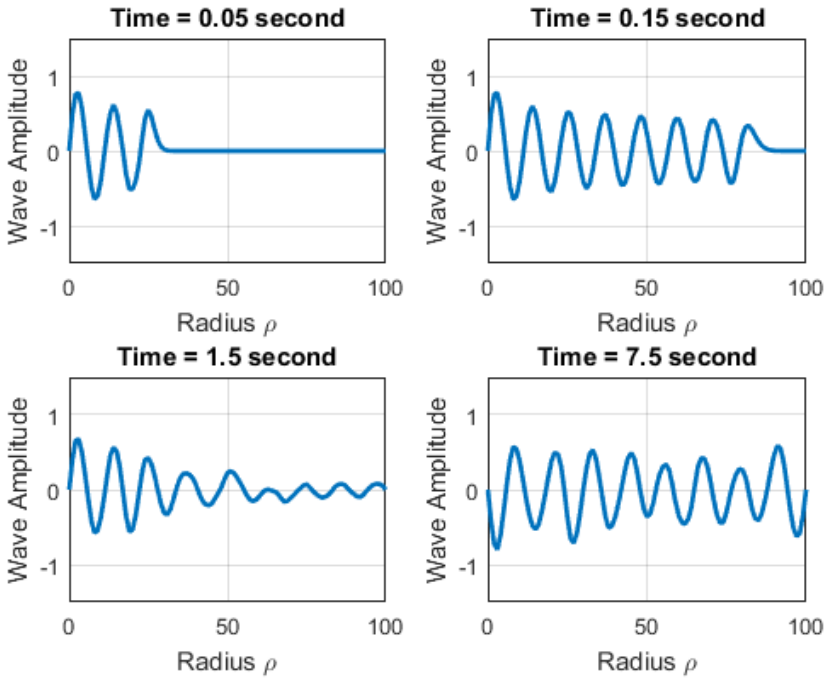

Figure 3.4: Time-domain representation of wave propagation in the exponential spiral string at several time instances.

Since we have access to the time-domain data at all spatial positions on the string, we easily calculated the frequency spectrum of the output wave at $\rho = L - 1 = 99$, where we considered the set of boundary conditions of $\psi(\rho = 0, t) = 1$ at constant input and $\psi(\rho = L, t) = 0$ at the fixed end. Figure 3.5 displays the resonance modes in an exponential spiral string of length $L = 100$. The spectrum provides the important fact that the resonance modes are not harmonics of integer multiples of a fundamental frequency. However each two consecutive modes have approximately a constant frequency difference of $2.9Hz$. More important than the ratio of the modes to each other, the fact that the system introduces inharmonicity is significant in terms of Musical acoustics.

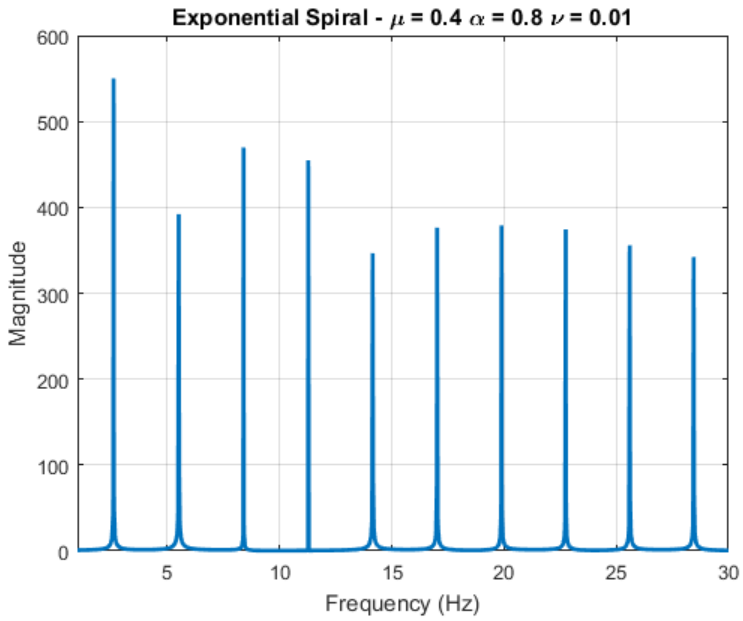

Figure 3.5: Exponential spiral string output resonance mode ($\rho = 99$). The first six mode frequencies are: $2.61, 5.51, 8.4, 11.28, 14.15, 17.02Hz$

3.2.2 Conical spiral string

We proceed with a similar method used for the exponential spiral. We define the spiral and height profiles as $\rho = \alpha\theta$ and $z = \beta\rho$. Therefore $\frac{\partial^2\psi}{\partial\theta^2} = \alpha^2\frac{\partial^2\psi}{\partial\rho^2}$ and $\frac{\partial^2\psi}{\partial z^2} = \frac{1}{\beta^2}\frac{\partial^2\psi}{\partial\rho^2}$. Equation 97 can be re-written as:

$$f(\rho)\frac{\partial^2\psi}{\partial\rho^2} + \frac{1}{\rho}\frac{\partial\psi}{\partial\rho} - \frac{1}{c^2}\frac{\partial^2\psi}{\partial t^2} - \frac{\nu}{c^2}\frac{\partial\psi}{\partial t} = 0 \tag{112}$$

where $f(\rho) = \frac{1}{\beta^2} + \frac{\alpha^2}{\rho^2} + 1$. Applying the same central difference scheme will result in:

$$\psi_n^{k+1} = \frac{c_2(n)}{c_1}\psi_{n+1}^k + \frac{c_3(n)}{c_1}\psi_n^k + \frac{c_4(n)}{c_1}\psi_{n-1}^k + \frac{c_5}{c_1}\psi_n^{k-1} \tag{113}$$

$$c_1 = \frac{1}{(c\Delta t)^2} + \frac{\nu}{2\Delta t c^2} \qquad c_2(n) = \frac{1}{2n\Delta\rho^2} + \frac{f(\rho_n)}{\Delta\rho^2} \tag{114}$$

$$c_3(n) = -2\frac{f(\rho_n)}{\Delta\rho^2} + \frac{2}{(c\Delta t)^2} \qquad c_4(n) = -\frac{1}{2n\Delta\rho^2} + \frac{f(\rho_n)}{\Delta\rho^2} \tag{115}$$

$$c_5 = -\frac{1}{(c\Delta t)^2} + \frac{\nu}{2\Delta t c^2} \tag{116}$$

However we need the value of ψ_n^{-1} to evaluate ψ_n^1, which by using the initial velocity condition approximation, we obtain:

$$\psi_n^1 = \frac{\frac{c_2(n)}{c_1}\psi_{n+1}^0 + \frac{c_3(n)}{c_1}\psi_n^0 - 2\frac{c_5(n)}{c_1}\Delta t g(r_n)}{1 - \frac{c_5(n)}{c_1}} \tag{117}$$

We used the same space and time mesh parameters as for the exponential spiral case.

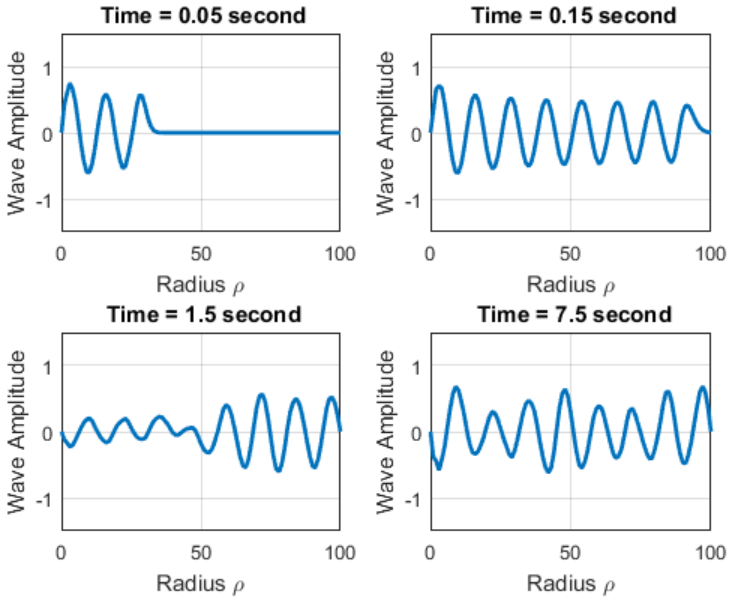

Figure 3.6: Time-domain representation of wave propagation in the conical spiral string at several time instances.

It can be seen from the output spectrum that the resonance modes of the conical spiral string are neither harmonic, where each two consecutive mode have a frequency difference of $3.2Hz$. Thus this system also produces inharmonicity and not immediately suitable for musical applications.

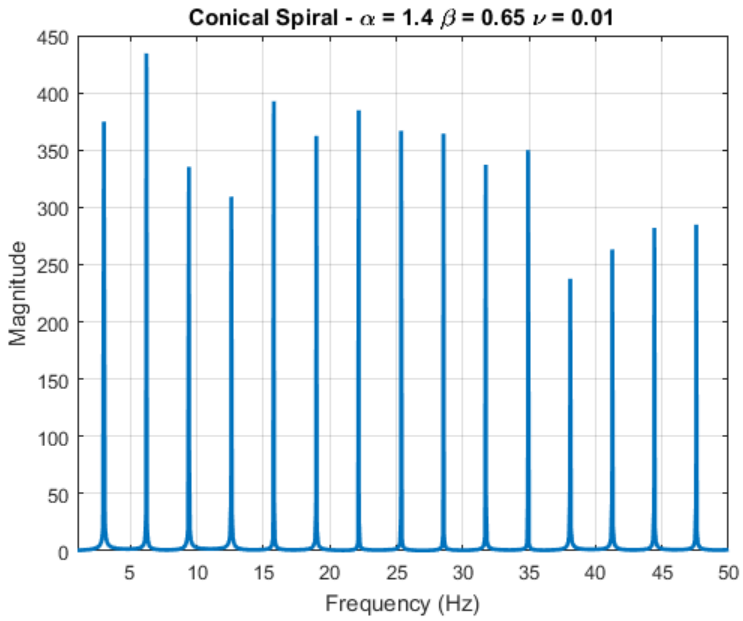

Figure 3.7: Conical spiral string output resonance mode ($\rho = 99$). The first six mode frequencies are: $2.99, 6.19, 9.39, 12.58, 15.78, 18.98Hz$

The numerical simulation MATLAB codes for both the conical and exponential spiral strings are provided in Appendix A.

3.3 Exponential spiral tube - Webster's horn equation

We previously saw that Rath and Naik [11] derived Webster's horn equation for a conical spiral geometry since the conch shell cavity is more accurately modelled as a tube with a cross-section rather than a wrapped string. Here we attempt to follow the same method for an exponential spiral tube (assuming harmonic motion). We will assume the cross-section of the tube to have a circular profile.

We assume the spiral passing through the center of the cross-section of the tube defined by $\rho = \alpha e^{\mu\theta}$. Therefore the outer and inner spirals may be defined as $\rho_1 = (\alpha+\delta)e^{\mu\theta}$ and $\rho_2 = (\alpha-\delta)e^{\mu\theta}$. Therefore the cross-section radius can be obtained from $\frac{\rho_1-\rho_2}{2} = \delta e^{\mu\theta}$. We also define the height profile as $\xi = \beta z$ thus defining a small height difference as $d\xi = \beta dz$, the total cross-section area

will be equal to:

$$S = \pi(\delta^2 e^{2\mu\theta} + \beta^2 z^2) \tag{118}$$

Substituting S into Webster's horn equation gives us:

$$\frac{\partial^2\psi}{\partial\rho^2} + \frac{1}{\rho}\frac{\partial\psi}{\partial\rho} + \frac{1}{\rho^2}\frac{\partial^2\psi}{\partial\theta^2} + \frac{\partial^2\psi}{\partial z^2} + \frac{1}{\rho^2}\frac{\partial\psi}{\partial\theta}\frac{2\mu\delta^2 e^{2\mu\theta}}{\delta^2 e^{2\mu\theta} + \beta'^2 z^2} + \frac{\partial\psi}{\partial z}\frac{2\beta'^2 z}{\delta^2 e^{2\mu\theta} + \beta'^2 z^2} + k^2\psi = 0 \tag{119}$$

In order to further simplify the equation, we assume that the spiral growth in the $x-y$ plane is much larger than in the z direction, i.e. $\delta^2 e^{2\mu\theta} \gg \beta^2 z^2$. Therefore we obtain:

$$\frac{\partial^2\psi}{\partial\rho^2} + \frac{1}{\rho}\frac{\partial\psi}{\partial\rho} + \frac{1}{\rho^2}\frac{\partial^2\psi}{\partial\theta^2} + \frac{2\mu}{\rho^2}\frac{\partial\psi}{\partial\theta} + \frac{\partial^2\psi}{\partial z^2} + k^2\psi = 0 \tag{120}$$

Assuming that the solution is separable and $\psi(\rho,\theta,z,t) = R(\rho)\Theta(\theta)Z(z)e^{j\omega t}$, equation 117 becomes:

$$\frac{1}{R}\frac{\partial^2 R}{\partial\rho^2} + \frac{1}{\rho R}\frac{\partial R}{\partial\rho} + \frac{1}{\rho^2\Theta}\frac{\partial^2\Theta}{\partial\theta^2} + \frac{2\mu}{\rho^2\Theta}\frac{\partial\Theta}{\partial\theta} + \frac{1}{Z}\frac{\partial^2 Z}{\partial z^2} + k^2 = 0 \tag{121}$$

The Z component solution can be derived from:

$$\frac{1}{Z}\frac{\partial^2 Z}{\partial z^2} = -l^2 \tag{122}$$

where if we assume the equation to have a solution of form $Z = e^{cz}$, it can be easily found that $Z = e^{\pm jlz}$. Inserting the Z solution back into equation 118 and multiplying the whole by ρ^2 gives:

$$\frac{\rho^2}{R}\frac{\partial^2 R}{\partial\rho^2} + \frac{\rho}{R}\frac{\partial R}{\partial\rho} + \frac{1}{\Theta}\frac{\partial^2\Theta}{\partial\theta^2} + \frac{2\mu}{\Theta}\frac{\partial\Theta}{\partial\theta} + \rho^2(k^2 - l^2) = 0 \tag{123}$$

The Θ component of the solution can be found from:

$$\frac{1}{\Theta}\frac{\partial^2\Theta}{\partial\theta^2} + \frac{2\mu}{\Theta}\frac{\partial\Theta}{\partial\theta} = -p^2 \tag{124}$$

Multiplying by Θ gives:

$$\frac{\partial^2\Theta}{\partial\theta^2} + 2\mu\frac{\partial\Theta}{\partial\theta} + p^2\Theta = 0 \tag{125}$$

Assuming that $\mu > \alpha$, the solution for equation 122 becomes:

$$\Theta(\theta) = e^{(-\mu \pm \sqrt{\mu^2 - \alpha^2})\theta} \tag{126}$$

Finally the radial solution can be derived as we substitute the Θ solution into equation 120:

$$\frac{\rho^2}{R}\frac{\partial^2 R}{\partial \rho^2} + \frac{\rho}{R}\frac{\partial R}{\partial \rho} + (\rho^2(k^2 - l^2) - p^2) = 0 \tag{127}$$

Multiplying by R gives:

$$\rho^2\frac{\partial^2 R}{\partial \rho^2} + \rho\frac{\partial R}{\partial \rho} + (\rho^2(k^2 - l^2) - p^2)R = 0 \tag{128}$$

Based on Bowman's formulation of the Bessel differential equation, we finally can find the radial and thus the complete solution:

$$R(\rho) = AJ_p(\sqrt{k^2 - l^2}\rho) + BY_p(\sqrt{k^2 - l^2}\rho) \tag{129}$$

where A and B are constants. The complete solution is given as the product of the independent functions R, Θ, Z and $e^{j\omega t}$:

$$\psi = (AJ_p(\sqrt{k^2 - l^2}\rho) + BY_p(\sqrt{k^2 - l^2}\rho))e^{(-\mu \pm \sqrt{\mu^2 - \alpha^2})\theta}e^{\pm jlz}e^{j\omega t} \tag{130}$$

The evaluation of the constants A and B heavily depend on the applied boundary conditions.

Chapter 4

Conclusions and Future Work

4.1 Summary of the Work

In this thesis we first provided an overview of how resonance modes are created in cylindrical, conical and exponential bores as they nearly make up the majority of tubes used in crafting musical instruments. Then we conducted a geometrical modelling of a sample conch shell inner cavity with X-ray tomography scans, based on early studies by Bhat et al. [6] [7] Furthermore, we conducted spectrum analysis and directivity measurements on the conch shell where the shell was excited in three different ways (Lip-vibration, Loudspeaker and Electro-pneumatic transducer). We also reviewed two different theoretical acoustic models of the conch shell by Rath and Naik [9] [11] where the time independent Helmholtz equation was derived for the given spiral geometry, as well as the derivation of Webster's horn equation for a conical spiral tube. A similar study was also done by Chatterjee and Nayak [13] where we extended their work to the general case of a 3-D spiral of conical and exponential profiles. We numerically simulated the wave propagation in such geometries with finite difference techniques and computed the output spectra of such systems. We finally applied Rath and Naik's study on modelling using the Webster's horn equation to an exponential spiral tube.

4.2 Conclusions

Based on the analytical and experimental investigations described in the previous chapters, we draw the following conclusions:

(1) The inner cavity of a conch shell can be acoustically modelled as a wrapped conical bore due to similar acoustic properties, as well as the conical tube profile once the inner cavity is mathematically unwrapped.

(2) The inner cavity growth of the conch shell displays signs of the Fibonacci pattern.

(3) The shell produces clear harmonics when excited adaptively by player's lips, and we correlated the recorded spectrum resonance modes to the theoretical mode estimations with acceptable correspondence. However the shell input impedance was found to be non-harmonic.

(4) The directivity measurements suggest that the shell is an omni-directional sound radiator (transmitting signals uniformly in all directions) near its cavity resonance, explaining why it was often used in the past for signalling purposes.

(5) Based on the numerical analysis, the 3-D exponential and conical spiral strings exhibit inharmonicity and thus the output is not suitable for musical applications.

(6) A general solution to the exponential spiral tube model based on Webster's horn equation is derived but with constants to be evaluated with appropriate boundary conditions.

4.3 Future Work

The investigations described in this thesis open the scope for new and further investigations:

(1) Finite element modelling (FEM) of wave propagation inside a conch shell with its cross-section geometrical irregularities being taken into consideration.

(2) Further theoretical derivations to the solution to the exponential spiral tube case need to be done, with numerical simulation being carried out.

(3) It was explained how the shell recordings were carried out in a semi-anechoic chamber. An interesting idea is to evaluate the conch shell sound when the shell is played in open space where factors such as reverberation and background noise will play an important role in how the sound is perceived.

(4) Use of conch shell drivers in reverberation chambers could be explored.

(5) Use of conch shell loudspeakers in public address applications could be explored in view of its uniform directivity.

Appendix A

MATLAB Codes

A.0.1 Geometrical Modelling

t_height_radius.m

```
% Rasoul M.P. Aghdam
% MIE Department - Concordia University
% 2014-2016

%%% Height-Radius profile of the conch shell cavity %%%

clear all
close all
clc

R = [10.577 12.970 17.269 21.692 27.678 35.483 43.206]/10; % Radii
H = [58.225 55.316 48.373 41.079 27.604 19.506 0]/10; % Height

Rtop = [12.970 21.692 35.483]/10;
Rbot = -[10.577 17.269 27.678 43.206]/10;
```

```
16
17 Htop = [55.316 41.079 19.506]/10;
18 Hbot = [58.225 48.373 27.604 0]/10;
19
20 figure
21 hold on
22 [xData, yData] = prepareCurveData( Rbot, Hbot );
23 ft = fittype( 'poly2' );
24 [fitresult, gof] = fit( xData, yData, ft );
25 h = plot( fitresult, xData, yData );
26 set(h,'linewidth',1.5)
27
28 [xData2, yData2] = prepareCurveData( Rtop, Htop );
29 ft2 = fittype( 'poly2' );
30 [fitresult2, gof2] = fit( xData2, yData2, ft2 );
31 h2 = plot( fitresult2, xData2, yData2 );
32 set(h2,'linewidth',1.5)
33 xlabel('Radius (cm)')
34 ylabel('Height (cm)')
35 title('Second order polynomial fit to radius and height data')
36 grid on
```

t_spiralfit.m

```
1 % Rasoul M.P. Aghdam
2 % MIE Department - Concordia University
3 % 2014-2016
4
5 %%% Spiral fit to the conch shell spiral cavity %%%
6
```

```
close all
clear all
clc

R = [10.577 12.970 17.269 21.692 27.678 35.483 43.206]/10;
thetaP = [0 pi 2*pi 3*pi 4*pi 5*pi 6*pi];
theta1 = 0:0.01:4*pi-0.01;
theta2 = 4*pi:0.01:6*pi;
r1 = 0.125*theta1 + 10.577/10;
r2 = 0.225*theta2;

polar(thetaP,R,'s')
hold on
polar(theta1, r1 ,'o')
polar(theta2, r2 ,'o' )
title('Conical spiral fit to the conch shell 2-D cavity')
```

t_spirallength.m

```
% Rasoul M.P. Aghdam
% MIE Department - Concordia University
% 2014-2016

%%% Computation of the conch shell spiral length %%%

clear all
close all
clc

```

```
11 % Constants in the second order polynomial relating the spiral
       height and
12 % radius - z(r) = p1*r^2 + p2*r + p3 => dz(r) = 2*p1*r + p2
13 p1 = -0.07913;
14 p2 = -1.331;
15 p3 = 7.342;
16
17 theta1 = 0:4*pi-0.01;
18 r1 = 0.125*theta1 + 10.577/10;
19 theta2 = 4*pi:6*pi;
20 r2 = 0.225*theta2;
21
22 L1 = @(theta1) sqrt(((0.125*theta1 + 10.577/10).*cos(theta1)).^2
       + ((0.125*theta1 + 10.577/10).*sin(theta1)).^2 + (2*p1*(0.125*
       theta1 + 10.577/10) + p2).^2);
23 L2 = @(theta2) sqrt(((0.225*theta2).*cos(theta2)).^2 + ((0.225*
       theta2).*sin(theta2)).^2 + (2*p1*(0.225*theta2) + p2).^2);
24
25 % piecewise calculation of the spiral length
26
27 Len1 = integral(L1,0,4*pi-0.01);
28 Len2 = integral(L2,4*pi,6*pi);
29
30 L = Len1+Len2;
31 disp(L);
```

t_vertical_radius.m

```
1 % Rasoul M.P. Aghdam
2 % MIE Department - Concordia University
```

```
3 % 2014-2016
4
5 %%% Conch shell spiral cavity vertical radius profile as a
      function of cavity length %%%
6
7 clear all
8 close all
9 clc
10
11 TopR = [8.097 10.621 15.317 16.114 21.751 28 36.502]/10;
12 BotR = -[8.016 10.335 11.744 16.683 20.158 27.112 49.596]/10;
13
14 Len = [0 6.19 13.39 21.63 30.98 42.52 56.18];
15
16 hold on
17 [xData, yData] = prepareCurveData( Len, TopR );
18 ft = fittype( 'poly2' );
19 [fitresult, gof] = fit( xData, yData, ft );
20 h = plot( fitresult, xData, yData );
21 set(h,'linewidth',1.5);
22
23 [xData2, yData2] = prepareCurveData( Len, BotR );
24 ft2 = fittype( 'poly2' );
25 [fitresult2, gof2] = fit( xData2, yData2, ft2 );
26 h2 = plot( fitresult2, xData2, yData2 );
27 set(h2,'linewidth',1.5);
28 xlabel('Cavity␣Length␣(cm)')
29 ylabel('Radius␣(cm)')
```

```
30 grid on
31 title('Cross-section major (vertical) axis profile')
```

t_horizontal_radius.m

```
1 % Rasoul M.P. Aghdam
2 % MIE Department - Concordia University
3 % 2014-2016
4
5 %%% Horizontal radius profile as a function of the cavity length
      %%%
6
7 close all
8 clear all
9 clc
10
11 RightR = [2.699 3.619 3.849 6.698 7.328 8.687 12.422]/10;
12 LeftR = -[4.469 6.249 6.704 9.047 10.188 14.305 14.656]/10;
13
14 Len = [0 6.19 13.39 21.63 30.98 42.52 56.18]; % Spiral length at
      each turn
15
16 hold on
17 [xData, yData] = prepareCurveData( Len, RightR );
18 ft = fittype( 'poly2' );
19 [fitresult, gof] = fit( xData, yData, ft );
20 h = plot( fitresult, xData, yData );
21 set(h,'linewidth',1.5)
22
23 [xData2, yData2] = prepareCurveData( Len, LeftR );
```

```
ft2 = fittype( 'poly2' );
[fitresult2, gof2] = fit( xData2, yData2, ft2 );
h2 = plot( fitresult2, xData2, yData2 );
set(h2,'linewidth',1.5)
xlabel('Cavity Length (cm)')
ylabel('Radius (cm)')
grid on
title('Cross-section minor (horizontal) axis profile')
```

A.0.2 Numerical Simulation

t_bessel.m

```
% Rasoul M.P. Aghdam
% MIE Department - Concordia University
% 2014-2016

%%% Solution to the time-independent wave equation derived for a
    3-D exponential spiral string %%%

close all
clear all
clc

f = 100; % frequency
omega = 2*pi*f;

mu = 0.4;
alpha = 1.3;
lambda = (1 + mu^2)/(1 + mu^2 + 1/alpha^2);
```

```
17 p = (lambda - 1)/2;
18 c = 347; % wave velocity
19 k = omega/(c*sqrt(1 + mu^2 + 1/alpha^2));
20
21 ri = 0.5;
22 r0 = 100;
23 r = ri:0.01:r0;
24
25 c2 = 1/((ri^(-p))*(bessely(p,k*ri) - (bessely(p,k*r0)/besselj(p,k
       *r0))*besselj(p,k*ri)));
26 c1 = -c2*(bessely(p,k*r0)/besselj(p,k*r0));
27
28 y = (r.^(-p)).*(c1*besselj(p,k*r) + c2*bessely(p,k*r));
29
30 plot(r,y,'linewidth',1.5);
31 grid on
32 axis tight
33 xlabel('Radius')
34 ylabel('Solution')
35 % savefig('fig');
36 title('\mu = 0.4, \alpha = 1.3, f = 100Hz')
37
38 figure(2)
39 ri = 0.1;
40 r0 = 1;
41 hold on
42 for alpha = 1:0.1:2
43     n = 0.1:0.01:5;
```

```
44        mu2 = (1./(2*pi*n))*log(r0/ri);
45        out = 1./(1+mu2.^2+1/alpha^2);
46        grid on
47        xlabel('n')
48        ylabel('(\kappa/k)^2')
49        plot(n,out,'linewidth',1.25)
50        title('Variation of taper factor \alpha, r_m = 1, r_t = 0.1')
51  end
```

t_conical.m

```
1  % Rasoul M.P. Aghdam
2  % MIE Department - Concordia University
3  % 2014-2016
4
5  %%% Numerical simulation of wave propagation in a 3-D conical
       spiral string %%%
6
7  close all; clear all; clc;
8
9  % space mesh %
10 Nx = 101;
11 dx = 1; % space-step
12 x = (0:Nx-1)*dx;
13
14 % time mesh %
15 T = 100001; % total number of time steps
16 dt = 0.001; % time-Step
17 t = (0:T-1)*dt;
18
```

```
19 c = 347.23; % wave velocity
20 nu = 0.01; % wave damping
21 alpha = 1.4; % spiral scale
22 beta = 0.65; % spiral z scale
23 f = 50; % sine input frequency
24 s = T/f;
25
26 u = zeros(T,Nx); % solution initialization
27 % u(:,1) = ones(T,1); % boundary condition at x=0
28 u(1:s,1) = sin(2*pi*f*t(1:s)); % sine input boundary condition at
       x=0
29 v0 = 0; % initial velocity condition g(x)
30
31 % equation constants %
32 fn = 1 + 1/(beta^2) + (alpha^2)./(x.^2); % vector
33 c1 = 1/((c*dt)^2) + nu/(2*dt*c^2);
34 c2 = fn/(dx^2) + 1./(2*x*dx); % vector
35 c3 = -2*fn/(dx^2) + 2/((c*dt)^2); % vector
36 c4 = fn/(dx^2) - 1./(2*x*dx); % vector
37 c5 = -1/((c*dt)^2) + nu/(2*(c^2)*dt);
38
39 % CTCS finite difference scheme %
40
41 for i = 2:Nx-1
42     u(2,i) = ((c2(i)/c1).*u(1,i+1) + (c3(i)/c1).*u(1,i) + (c4(i)/
          c1).*u(1,i-1) - 2*dt*(c5/c1).*v0)/(1-c5/c1);
43 end
44
```

```
45 for j = 2:T-1
46     for i = 2:Nx-1
47         u(j+1,i) = (c2(i)/c1).*u(j,i+1) + (c3(i)/c1).*u(j,i) + (
               c4(i)/c1).*u(j,i-1) + (c5/c1)*u(j-1,i);
48     end
49 end
50 %-------------------------------------------------------------------%
51
52 plot_times = [51 151 1501 7501];
53
54 for i = 1:4
55
56     hold on;
57     subplot(2,2,i);
58     k = plot_times(i);
59     plot(x,u(k,:),'linewidth',2);
60     grid on;
61     axis([min(x) max(x) -1.5 1.5]);
62     xlabel('Radius \rho');
63     ylabel('Wave Amplitude');
64     titlestring = ['Time = ',num2str(t(k)), ' second'];
65     title(titlestring);
66     %   h=gca;
67     %   get(h,'FontSize')
68     %   set(h,'FontSize',14);
69     %   fh = figure(i);
70     %   set(fh, 'color', 'white');
71
```

```
72
73 end
74 %-------------------------------------------------------------------------%
75 % Movie for the travelling wave
76
77 % for j = 1:T
78 %     plot(x,u(j,:),'linewidth',2);
79 %     grid on;
80 %     axis([min(x) max(x) -2 2]);
81 %     xlabel('Radius \rho','fontSize',14);
82 %     ylabel('Wave Amplitude','fontSize',14);
83 %     titlestring = ['Time step = ',num2str(j), ' Time = ',num2str(
       t(j)), 'second'];
84 %     title(titlestring ,'fontsize',14);
85 %     h=gca;
86 %     get(h,'FontSize')
87 %     set(h,'FontSize',14);
88 %     fh = figure(5);
89 %     set(fh, 'color', 'white');
90 %     F=getframe;
91 %
92 % end
93 %
94 % movie(F,T)
95 %-------------------------------------------------------------------------%
96
97 % E = surf(x,t,u)
98 % E.LineStyle = ':'
```

```
99  % %E.EdgeColor = 'none'
100 % colormap hsv
101 % lighting gouraud
102 % material shiny
103 % xlabel('Distance')
104 % ylabel('Time (s)')
105 % zlabel('Amplitude')
106
107 % frequency domain plotting %
108 % vec = u(:,100);
109 % Y = fft(vec);
110 % T = length(vec);
111 % P2 = abs(Y/T);
112 % P1 = P2(1:floor(T/2)+1);
113 % P1(2:end-1) = 2*P1(2:end-1);
114 % Fs = 1/dt; % sampling frequency
115 % fq = [ 0: Fs/(T-2) : Fs/2 ];
116 % % plot(fq(1:250),P1(1:250));
117 % plot(fq,abs(Y(1:T/2)),'LineWidth',2);
118 % xlim([1 50]);
119 % grid on
120 % xlabel('Frequency (Hz)');
121 % ylabel ('Magnitude');
122 % title (['Conical Spiral - \alpha = ', num2str(alpha),' \beta =
        ', num2str(beta),' \nu = ', num2str(nu)]);
```

t_exponential.m

```
1 % Rasoul M.P. Aghdam
2 % MIE Department - Concordia University
```

```
3  % 2014-2016
4
5  %%% Numerical simulation of wave propagation in a 3-D exponential
       spiral string %%%
6
7  close all; clear all; clc;
8
9  % space mesh %
10 Nx = 101;
11 dx = 1; % space-step
12 x = (0:Nx-1)*dx;
13
14 % time mesh %
15 T = 100001; % total number of time steps
16 dt = 0.001; % time-Step
17 t = (0:T-1)*dt;
18
19 c = 347.23; % wave velocity
20 mu = 0.4; % spiral growth factor
21 nu = 0.01; % wave damping
22 alpha = 0.8; % spiral z scale
23 f = 50; % sine input frequency
24 s = T/f;
25
26 u = zeros(T,Nx); % solution initialization
27 % u(:,1) = ones(T,1); % boundary condition at x=0
28 u(1:s,1) = sin(2*pi*f*t(1:s)); % sine input boundary condition at
       x=0
```

```
29 v0 = 0; % initial velocity condition g(x)
30
31 % equation constants %
32 lambda = (1 + mu^2)/(1 + mu^2 + 1/alpha^2);
33 zeta = 1/(c^2*(1 + mu^2 + 1/alpha^2));
34 eta = nu*zeta;
35 c0 = zeta/dt^2 - eta/(2*dt);
36 c1 = -1/((dx^2)*c0);
37 c2 = -lambda/(2*(dx^2)*c0);
38 c3 = -zeta/((dt^2)*c0);
39 c4 = -eta/(2*dt*c0);
40
41 % CTCS finite difference scheme %
42
43 for i = 2:Nx-1
44     u(2,i) = u(1,i+1)*(-c1/(1-c3+c4) - c2/(i*(1-c3+c4))) + u(1,i)
          *(2*c1-2*c3)/(1-c3+c4) + u(1,i-1)*(-c1/(1-c3+c4) + c2/(i
          *(1-c3+c4))) + 2*dt*v0*(c4-c3)/(1-c3+c4);
45 end
46
47 for j = 2:T-1
48     for i = 2:Nx-1
49         u(j+1,i) = -c1*(u(j,i+1)-2*u(j,i)+u(j,i-1)) - (c2/i)*(u(j
              ,i+1) - u(j,i-1)) - 2*c3*u(j,i) + u(j-1,i)*(c3-c4);
50     end
51 end
52 %-------------------------------------------------------------------------%
53
```

```
54 plot_times = [51 151 1501 7501];
55
56 for i = 1:4
57
58   hold on
59   subplot(2,2,i);
60   k = plot_times(i);
61   plot(x,u(k,:),'linewidth',2);
62   grid on;
63   axis([min(x) max(x) -1.5 1.5]);
64   xlabel('Radius \rho');
65   ylabel('Wave Amplitude');
66   titlestring = ['Time = ',num2str(t(k)), ' second'];
67   title(titlestring);
68 %   h=gca;
69 %   get(h,'FontSize')
70 %   set(h,'FontSize',14);
71 %   fh = figure(i);
72 %   set(fh, 'color', 'white');
73 %
74 end
75 %-------------------------------------------------------------------------%
76 % Movie for the travelling wave
77
78 % for j = 1:T
79 %   plot(x,u(j,:),'linewidth',2);
80 %   grid on;
81 %   axis([min(x) max(x) -0.2 0.2]);
```

```
82 %     xlabel('X axis','fontSize',14);
83 %     ylabel('Wave Amplitude','fontSize',14);
84 %     titlestring = ['Time step = ',num2str(j), ' Time = ',num2str(
       t(j)), 'second'];
85 %     title(titlestring ,'fontsize',14);
86 %     h=gca;
87 %     get(h,'FontSize')
88 %     set(h,'FontSize',14);
89 %     fh = figure(5);
90 %     set(fh, 'color', 'white');
91 %     F=getframe;
92 %
93 % end
94 %
95 % movie(F)
96 %-------------------------------------------------------------------------%
97
98 % E = surf(x,t,u)
99 % E.LineStyle = ':'
100 % %E.EdgeColor = 'none'
101 % colormap hsv
102 % lighting gouraud
103 % material shiny
104 % xlabel('Distance')
105 % ylabel('Time (s)')
106 % zlabel('Amplitude')
107
108 % frequency domain plotting %
```

```
109 % vec = u(:,100);
110 % Y = fft(vec);
111 % T = length(vec);
112 % P2 = abs(Y/T);
113 % P1 = P2(1:floor(T/2)+1);
114 % P1(2:end-1) = 2*P1(2:end-1);
115 % Fs = 1/dt; % sampling frequency
116 % fq = [ 0: Fs/(T-2) : Fs/2 ];
117 %% plot(fq(1:250),P1(1:250));
118 % plot(fq,abs(Y(1:T/2)),'LineWidth',2);
119 % xlim([1 30]);
120 % grid on
121 % xlabel('Frequency (Hz)');
122 % ylabel ('Magnitude');
123 % title (['Exponential Spiral - \mu = ', num2str(mu),' \alpha =
        ', num2str(alpha),' \nu = ', num2str(nu)]);
```

Bibliography

[1] R.M. Pouraghdam and R.B. Bhat. Spectrum analysis and directivity pattern of a transducer-driven conch shell. *Canadian Acoustics*, 43(3):86–87, September 2015.

[2] N.H. Fletcher and T.D. Rossing. *The Physics of Musical Instruments*, chapter 2, pages 36–37. Springer, second edition, 1998.

[3] T.D. Rossing and N.H. Fletcher. *Principles of Vibration and Sound*, chapter 8, pages 175–176. Springer, second edition, 2004.

[4] N.H. Fletcher and T.D. Rossing. *The Physics of Musical Instruments*, chapter 8, pages 210–211. Springer, Second.

[5] H.F. Olson. *Acoustical Engineering*, pages 88–123. Van Nostrand-Reinhold, Princeton, New Jersey, 1957.

[6] R.B. Bhat. Acoustics of conch shells. *Journal of Sound and Vibration*, 157(1):190–191, 1992.

[7] L.R. Taylor M.G. Prasad and R.B. Bhat. Geometrical modeling and spectral analysis of a conch shell trumpet. *Third International Congress on Air And Structure-Borne Sound And Vibration*, June 1994.

[8] S.K. Rath and P.C. Naik. Fibonacci structure in conch shell. *Current Science*, 88(4):555–557, February 2005.

[9] S.K. Rath and P.C. Naik. A study on acoustics of conch shell. *Current Science*, 97(4):521–528, August 2009.

[10] L.J. Eliason D.R. Ayers and D. Mahgerefteh. The conical bore in musical acoustics. *American Journal of Physics*, 53(6):528–537, June 1985.

[11] S.K. Rath and P.C. Naik. On acoustic theory of conch shell. *Current Science*, 99(6):790–795, August 2010.

[12] B. Kolbrek. Horn theory: An introduction, part 1. Technical report, http://www.audioxpress.com, 2008.

[13] D. Chatterjee and K.R. Nayak. Wave propagation in 1-d spiral geometry. *arXiv:1410.4939 (physics.class-ph)*, 2014.

[14] D.H. Von Seggern. *CRC Standard Curves and Surfaces with Mathematica*, chapter 12, pages 464–465. Chapman and Hall/CRC, 2 edition, October 2006.

[15] R.S. Esfandiari. *Numerical Methods for Engineers and Scientists Using MATLAB*, chapter 6, pages 274–275. CRC Press, 2013.